

Interference Phenomena in Electronic Transport Through Chaotic Cavities: An Information-Theoretic Approach

Pier A. Mello[†] and Harold U. Baranger[‡]

[†] Instituto de Física, Universidad Nacional Autónoma de México, 01000 México D.F., México

[‡] Bell Laboratories– Lucent Technologies, 700 Mountain Ave. 1D-230, Murray Hill NJ 07974

1 December 1998

Abstract. We develop a statistical theory describing quantum-mechanical scattering of a particle by a cavity when the geometry is such that the classical dynamics is chaotic. This picture is relevant to a variety of physical systems, ranging from atomic nuclei to mesoscopic systems to microwave cavities; the main application here is to electronic transport through ballistic microstructures. The theory describes the regime in which there are two distinct time scales, associated with a prompt and an equilibrated response, and is cast in terms of the matrix of scattering amplitudes S . The prompt response is related to the energy average of S which, through the notion of ergodicity, is expressed as the average over an ensemble of similar systems. We use an information-theoretic approach: the ensemble of S -matrices is determined by (1) general physical features— symmetry, causality, and ergodicity, (2) the specific energy average of S , and (3) the notion of minimum information in the ensemble. This ensemble, known as Poisson’s kernel, is meant to describe those situations in which any other information is irrelevant. Thus, one constructs the one-energy statistical distribution of S using only information expressible in terms of S itself without ever invoking the underlying Hamiltonian. This formulation has a remarkable predictive power: from the distribution of S we derive properties of the quantum conductance of cavities, including its average, its fluctuations, and its full distribution in certain cases, both in the absence and presence prompt response. We obtain good agreement with the results of the numerical solution of the Schrödinger equation for cavities in which the assumptions of the theory hold: ones in which either prompt response is absent or there are two widely separated time scales. Good agreement with experimental data is obtained once temperature smearing and dephasing effects are taken into account.

Contents

1	Introduction	3
1.1	The atomic nucleus and microwave cavities	3
1.2	Ballistic Mesoscopic Cavities	4
2	The scattering problem	5
2.1	Scattering waves: Definition of the S -matrix	5
2.2	The conductance	7
2.3	Polar representation of the S matrix	7
3	Ensembles of S matrices: An information-theoretic approach	8
3.1	The invariant measure	8
3.2	The information-theoretic model	9
3.2.1	The one-channel case	9
3.2.2	The multi-channel case	10
4	Absence of direct processes	12
4.1	Averages of products of S : Weak-localization and conductance fluctuations	12
4.1.1	The case $\beta=2$	12
4.1.2	The case $\beta=1$	14
4.2	The distribution of the conductance in the two-equal-lead case	16
4.2.1	The case $N=1$	16
4.2.2	The case $N=2$	16
4.2.3	The case $N=3$	16
4.2.4	Arbitrary N	16
5	Presence of direct processes	17
5.1	The case $\beta=2$	17
5.2	The case $\beta=1$	18
6	Comparison with numerical calculations	18
6.1	Simple structures	19
6.2	Absence of direct processes	21
6.3	Presence of direct processes	22
7	Comparison with experimental data: Dephasing effects	24
7.1	Large N_ϕ	25
7.2	Arbitrary N_ϕ	27
7.3	Experiment	28
8	Conclusion	29
A	Appendix: Evaluation of the invariant measure	31
A.1	The case $\beta=1$	32
A.2	The case $\beta=2$	34
B	Appendix: The distribution of the conductance in the absence of direct processes	35
B.1	Derivation of Eq.(4.42).	35
B.2	Derivation of Eq. (4.41)	36
B.3	Derivation of Eq. (4.44)	36

1. Introduction

Scattering of waves by complex systems has captured the interest of physicists for a long time. For instance, the problem of multiple scattering of waves has been of great importance in optics [1,2]. Interest in this problem has been revived recently, both for electromagnetic waves [3] and for electrons [4], in relation with the phenomenon of localization, which gives rise to a great many fascinating effects.

Nuclear physics, with typical dimensions of a few fm ($1\text{ fm} = 10^{-15}\text{ m}$), offers excellent examples of quantum-mechanical scattering by “complex” many-body systems dating as far back as the 1930’s when compound-nucleus resonances were discovered [5]. The treatment in these cases is often frankly statistical because the details of the many-body problem are intractably complicated.

In the last two decades, electron transport in disordered metals has been intensively investigated [4,6,7,8,9,10], as has transmission of electromagnetic waves through disordered media [3,4,7]. The typical size scale is $1\mu\text{m}$ for electronic systems and $1\mu\text{m}$ to 0.1m in the electromagnetic case. Because these are also examples of scattering in complex environments, where the character of the disorder is not exactly known, a statistical approach which treats an ensemble of disordered potentials is natural.

Amazingly, features similar to those of these complex nuclear and disordered problems have also been found in certain “simple” systems. While the geometry of these systems is apparently very simple—quantum-mechanical scattering of just one particle by three circular disks in a plane, for instance—the classical dynamics is fully chaotic. Such systems have been studied by the “quantum chaos” community, in which the main question is how the nature of the classical dynamics influences the quantum properties [11,12]. In contrast to the complex cases, these systems are amenable to exact (numerical) calculation; when the results are analyzed statistically, however, the results are closely related to those of the complex systems [11,12]. Experimentally, two types of simple scattering systems have been studied in particular: electron transport through microstructures called “ballistic quantum dots”, whose dimensions are of the order of $1\mu\text{m}$, and microwave scattering from metallic cavities, with typical dimensions of 0.1m .

The “universal” statistical properties of wave-interference phenomena observed in systems whose dimensions span about 14 orders of magnitude turn out to depend on very general physical principles and constitute the central topic of this article. Although our main interest throughout the paper is electronic transport through ballistic chaotic cavities, or ballistic quantum dots, described in section 1.2, we wish to emphasize the generality of the ideas involved, presenting first in section 1.1 their application in the field of nuclear physics—where some of them were first introduced—with a brief reference to microwave cavities at the end of that subsection.

1.1. The atomic nucleus and microwave cavities

One of the most successful models in nuclear physics, called the optical model of the nucleus, was invented by Feshbach, Porter and Weisskopf in the 1950’s [13,14]. That model, which works very nicely over a wide range of energies, describes the scattering of a nucleon by an atomic nucleus— a complicated many-body problem— in terms of two distinct time scales:

1. A *prompt* response arising from *direct processes*, in which the incident nucleon feels a mean field produced by the other nucleons. This response is described mathematically in terms of the *average* of the actual scattering amplitudes over an energy interval: these averaged amplitudes, also known as *optical* amplitudes, show a much slower energy variation than the original ones.

2. A *delayed*, or *equilibrated*, response, corresponding to the formation and decay of the compound nucleus. It is described by the difference between the exact and the optical scattering amplitudes: it varies appreciably with energy and is studied with *statistical* concepts using techniques known as random matrix theory [15,16].

Just as in the field of statistical mechanics time averages are very difficult to construct and hence are replaced by *ensemble averages* using the notion of *ergodicity*, in the present context too one finds it advantageous to study energy averages in terms of ensemble averages through an ergodic property [17,18,19,20].

The optical model not only works well in nuclear physics, but has also been applied successfully in the description of a number of chemical reactions, thus bringing us from the nuclear to the molecular

size scale [21].

The connection of the above problems with the theory of waveguides and cavities was proposed very clearly by Ericson and Mayer-Kuckuk more than thirty years ago [22]: “Nuclear-reaction theory is equivalent to the theory of waveguides... We will concentrate on processes in which the incident wave goes through a highly complicated motion in the nucleus... We will picture the nucleus as a closed cavity, with reflecting but highly irregular walls.”

In fact, recent experiments with microwave cavities have shown features similar to those that had been observed in the nuclear case. Importantly, the “irregular walls” anticipated from the nuclear case are *not* necessary in order to see these features: the analogy between nuclear reaction theory and the theory of waveguides holds for simple smooth cavities as long as the corresponding classical dynamics is chaotic [23,24,25]. This has been the focus of several recent experiments involving microwave scattering from metallic cavities [26,27,28,29]. These studies in simple chaotic systems were predated by extensive studies on scattering of microwaves by a disordered dielectric medium; particularly important are the experiments of A. Genack and collaborators [30]. It is also interesting to note that the use of statistical concepts to analyze electromagnetic scattering by waveguides started quite independently of the connection to the complex scattering of nuclear physics, in the context of radio wave propagation [31].

1.2. Ballistic Mesoscopic Cavities

The term *mesoscopic* system refers to microstructures in which the phase of the single-electron wave function— in an independent-electron approximation— remains coherent across the system of interest [4,6,7,8,9,10]: this means that the phase-coherence length l_ϕ associated with processes that can change the environment— the other electrons, or the phonon field— to an orthogonal state exceeds the system size [6]. This is realized in the laboratory with systems whose spatial dimensions are on the order of $1\mu\text{m}$ or less and at temperatures ≤ 1 K. In so-called *ballistic cavities*, or *quantum dots*, the electron motion is in addition practically ballistic, except for specular reflection from the walls: thus the elastic mean free path l_{el} also exceeds the system size. In the most favorable material system, GaAs heterostructures, this condition can also be realized for cavities of size $\leq 1\mu\text{m}$ [6,7,8,9].

Experimentally, an electrical current is established through the leads that connect the cavity to the outside and the potential difference across the cavity is measured, from which the conductance G is extracted. In an independent-electron picture one thus aims at understanding the quantum-mechanical single-electron scattering by the cavity, while the leads play the role of waveguides. It is the multiple scattering of the waves reflected by the various portions of the cavity that gives rise to interference effects. Three important experimental probes of the interference effects are an external magnetic field B , the Fermi energy ϵ_F , and the shape of the cavity: when these are varied the relative phase of the various partial waves changes and so the interference pattern changes. The changing interference pattern in turn causes the conductance to change; this sensitivity of G to small changes in parameters through quantum interference is called *conductance fluctuations*.

The connection between scattering by simple chaotic cavities [23,24,25] and mesoscopic systems was first made theoretically [32]. Subsequently, cavities in the shape of a stadium, for which the single-electron classical dynamics would be chaotic, were first reported in Ref. [33]. More recently, several other types of structures have been investigated including experimental *ensembles* of shapes [34,35,36,37,38,39,40,41,42,43,44]. Averages of the conductance, its fluctuations, and its full distribution were obtained over such an ensemble.

It is the aim of the present paper to provide a theoretical framework to describe this physical situation. To this end we will set up a scheme similar to that explained in section 1.1 in connection with the scattering problem in nuclear physics. A complementary treatment based on semiclassical ideas has also been developed but will not be covered here [32,45].

The paper is organized as follows. We start by presenting the general ideas of quantum-mechanical scattering by a cavity, introducing the scattering or S matrix of the problem (Sec. 2), and then turn to treating an ensemble of systems in terms of an ensemble of S matrices (Sec. 3). Specific analytical results for the conductance are then presented, first in the absence of direct processes (Sec. 4), and then with direct processes present (Sec. 5). We then compare our theoretical results with the numerical solution of the Schrödinger equation (Sec. 6), and finally in Sec. 7 compare with the experimental data

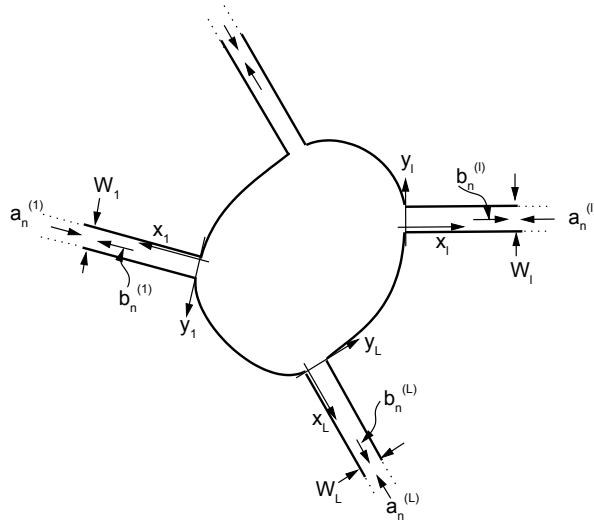


Figure 1. The 2D cavity studied in the text. The cavity is connected to the outside via L waveguides. The arrows inside the waveguides indicate incoming or outgoing waves as in Eq. (2.1). In waveguide l there can be N_l such incoming or outgoing waves: this is indicated in the figure by the amplitudes a_n^l , b_n^l , respectively, where $n=1, \dots, N_l$.

that were already mentioned above. In the latter comparisons, a number of discrepancies are found; to reconcile theory and experiment, we realize the necessity of introducing the effect of processes that destroy the coherence of the wave function in the sample. Finally, the conclusions of our work are presented in Sec. 8. Some of the main results in this paper have appeared in condensed form in our previous publications [46,47,48].

2. The scattering problem

2.1. Scattering waves: Definition of the S -matrix

Consider a system of noninteracting electrons. Since we shall be dealing with cases in which spin-orbit coupling is negligible, we disregard the spin degree of freedom and just consider “spinless electrons” in what follows. We are interested in studying the scattering of an electron at the Fermi energy $\epsilon_F = \hbar^2 k_F^2 / 2m$ by the 2D microstructure shown schematically in Fig. 1. The microstructure consists of a cavity, connected to the outside by L leads, ideally of infinite length, that play the role of waveguides. The l -th lead ($l=1, \dots, L$) has width W_l . We are interested in the (scattering) solutions of the Schrödinger equation *inside* such a structure, with the ideal boundary condition that the walls of the cavity and leads are completely impenetrable: hence the wave function must vanish there.

In each lead l we introduce a system of coordinates x_l, y_l , as indicated in Fig. 1. The x_l axis runs along the lead and points outwards from the cavity. The y_l axis runs in the transverse direction and is tangential to the cavity wall and its continuation across the lead; y_l takes on the values 0 and W_l on the two walls of the lead. In lead l and for $x_l > 0$ we have the elementary solutions to the Schrödinger equation

$$e^{\pm i k_n^{(l)} x_l} \chi_n(y_l) \quad (2.1)$$

where the positive (negative) sign is for outgoing (incoming) waves. Here the functions $\chi_n(y_l)$ are the solution of the transverse Hamiltonian which in the presence of a magnetic field may depend on $k_n^{(l)}$ [49]. The solution of the scattering problem consists in expressing the amplitude of the outgoing waves in terms of the incoming ones.

In the absence of a magnetic field, the explicit problem can be simply stated; we now present this case in detail, noting that it can be generalized to the $B \neq 0$ case [49]. For $B=0$, the functions $\chi_n(y_l)$

are

$$\chi_n(y_l) = \sqrt{\frac{2}{W_l}} \sin K_n^{(l)} y_l, \quad K_n^{(l)} = \frac{n\pi}{W_l}, \quad n=1, 2, \dots \quad (2.2)$$

where $K_n^{(l)}$ is the “transverse wave number”. The functions $\chi_n(y_l)$ vanish on the two walls of the lead and form a complete orthonormal set of functions for the variable y_l ; i.e.

$$\langle \chi_n | \chi_m \rangle = \delta_{nm}. \quad (2.3)$$

This “transverse quantization” is a consequence of the boundary condition on the walls of the leads. Each possibility defined by the integer n is named a *mode*, or *channel*. The “longitudinal” wave number $k_n^{(l)}$ satisfies the relation

$$[k_n^{(l)}]^2 + [K_n^{(l)}]^2 = k_F^2. \quad (2.4)$$

If $K_n^{(l)} < k_F$, then $[k_n^{(l)}]^2 > 0$, $k_n^{(l)}$ is real, and the $e^{\pm i k_n^{(l)} x_l}$ occurring in Eq. (2.1) represent running waves along the leads: we thus have *running modes* or *open channels*. On the other hand, when $K_n^{(l)} > k_F$, then $[k_n^{(l)}]^2 < 0$ and $k_n^{(l)}$ is pure imaginary, thus giving rise to exponentially decaying waves along the leads: these modes are called *evanescent modes* or *closed channels*. If

$$N_l < k_F W_l / \pi < N_l + 1, \quad (2.5)$$

there are N_l open channels in lead l . Very far away along the leads, i.e. as $x_l \rightarrow \infty$, only the contribution of the open channels contributes to the wave function. The most general form of the asymptotic wave function in lead l is thus the linear combination

$$\sum_{n=1}^{N_l} \left[a_n^{(l)} \frac{e^{-i k_n^{(l)} x_l}}{(\hbar k_n^{(l)} / m)^{1/2}} + b_n^{(l)} \frac{e^{i k_n^{(l)} x_l}}{(\hbar k_n^{(l)} / m)^{1/2}} \right] \chi_n(y_l). \quad (2.6)$$

Note that the normalization of the plane waves is such that they give rise to *unit flux*.

We define the N_l -dimensional vector

$$\mathbf{a}^{(l)} = (a_1^{(l)}, \dots, a_{N_l}^{(l)})^T \quad (2.7)$$

that contains the N_l incoming amplitudes in lead l ($l=1, \dots, L$). Putting all the $\mathbf{a}^{(l)}$ ($l=1, \dots, L$) together, we form the vector

$$\mathbf{a} = (\mathbf{a}^{(1)}, \dots, \mathbf{a}^{(L)})^T \quad (2.8)$$

associated with the incoming waves in all the channels for all the leads. We can make similar definitions for the outgoing-wave amplitudes. The *scattering matrix*, or *S matrix*, is then defined by the relation

$$\mathbf{b} = S \mathbf{a}, \quad (2.9)$$

connecting the incoming to the outgoing amplitudes. In terms of individual leads we can write

$$S = \begin{bmatrix} r_{11} & t_{12} & \dots & t_{1L} \\ t_{21} & r_{22} & \dots & t_{2L} \\ \vdots & \vdots & \ddots & \vdots \\ t_{L1} & t_{L2} & \dots & r_{LL} \end{bmatrix}. \quad (2.10)$$

Here, r_{ll} is an $N_l \times N_l$ matrix, containing the reflection amplitudes from the N_l channels of lead l back to the same lead; t_{lm} is an $N_l \times N_m$ matrix, containing the transmission amplitudes from the N_m channels of lead m to the N_l channels of lead l . The S matrix is thus a square matrix with dimensionality n given by

$$n = \sum_{l=1}^L N_l. \quad (2.11)$$

While we have carried out the analysis explicitly for $B=0$, the main results, Eqs. (2.1), (2.6), (2.9), and (2.10), also hold in the presence of a magnetic field.

Having chosen the unit-flux normalization for the plane waves in Eq. (2.6), *flux conservation* implies *unitarity* of the S matrix [1,50,51,52]; i.e.

$$SS^\dagger = I. \quad (2.12)$$

In the absence of other symmetries, we have this requirement only. This is the *unitary* case, also designated in the literature as $\beta = 2$. In the presence of *time-reversal invariance* (TRI) (as in the absence of a magnetic field) and no spin, the S matrix, besides being unitary, is *symmetric* [1,50,51,52,53]:

$$S = S^T \quad (2.13)$$

This is the *orthogonal* case, also designated as $\beta = 1$. The *symplectic* case ($\beta = 4$), arising in the presence of spin and time-reversal invariance, will not be touched upon in this presentation.

2.2. The conductance

For a two-lead problem, which will occur most frequently in our analysis, the S matrix has the structure

$$S = \begin{bmatrix} r_{11} & t_{12} \\ t_{21} & r_{22} \end{bmatrix} \equiv \begin{bmatrix} r & t' \\ t & r' \end{bmatrix}. \quad (2.14)$$

In the particular case $N_1 = N_2 = N$, i.e. when the two leads have the same number of channels N , the four blocks r, t, r', t' are $N \times N$ and the S matrix is $2N \times 2N$.

As we mentioned in the Introduction, we are interested in the electronic *conductance* of the microstructure. If we assume that the latter is placed between two reservoirs (at different chemical potentials) shaped as expanding horns with negligible reflection back to the microstructure, then the Landauer-Büttiker formula [57,58,59] expresses the conductance G in terms of the *scattering properties of the microstructure itself* as

$$G = \frac{e^2}{h} g, \quad g = 2T, \quad (2.15)$$

where the factor 2 arises from the two spin degrees of freedom and the “spinless conductance” T is the transmission coefficient $|t_{ab}|^2$ summed over initial and final channels:

$$T = \text{Tr}(tt^\dagger). \quad (2.16)$$

2.3. Polar representation of the S matrix

In the two-lead case with $N_1 = N_2 = N$, one can parametrize the S matrix in the so called “polar representation” as [54,55,56,46]

$$S = \begin{bmatrix} v_1 & 0 \\ 0 & v_2 \end{bmatrix} \begin{bmatrix} -\sqrt{1-\tau} & \sqrt{\tau} \\ \sqrt{\tau} & \sqrt{1-\tau} \end{bmatrix} \begin{bmatrix} v_3 & 0 \\ 0 & v_4 \end{bmatrix} = VRW. \quad (2.17)$$

Here, τ stands for the N -dimensional diagonal matrix of eigenvalues τ_a ($a=1, \dots, N$) of the Hermitian matrix tt^\dagger . The v_i ($i=1, \dots, 4$) are arbitrary $N \times N$ unitary matrices for $\beta=2$, with the restrictions

$$v_3 = v_1^T, \quad v_4 = v_2^T \quad (2.18)$$

for $\beta=1$. It is readily verified that any matrix of the form (2.17) satisfies the appropriate requirements of an S matrix for $\beta = 1, 2$. The converse statement, as well as the uniqueness of the polar representation, can also be proved using an argument similar to that in Ref. [55].

In the polar representation, we can write the total transmission T of Eq. (2.16) as

$$T = \sum_a \tau_a. \quad (2.19)$$

Thus the polar representation is natural for the study of conductance since it separates the magnitude of the transmission— the transmission eigenvalues $\{\tau_a\}$ — from the irrelevant phase effects— the unitary matrices $\{v_i\}$.

3. Ensembles of S matrices: An information-theoretic approach

As we mentioned in the Introduction, we are interested in ensembles of systems, which will be represented as *ensembles of S matrices* endowed with a *probability measure*. For that purpose it is important to introduce first the notion of *invariant measure* for our S matrices: this we develop in the first subsection. The second subsection is devoted to the derivation of the probability measure for our ensemble of S matrices, using an information-theoretic point of view.

3.1. The invariant measure

The invariant measure is the measure which equally weights all matrices which satisfy the unitarity and symmetry constraints. Intuitively, it corresponds to the most random distribution consistent with the constraints, or in other words the one with the least information. Mathematically, such a measure is defined by requiring that it remain invariant under an automorphism of a given symmetry class of matrices into itself [53,54]:

$$d\mu^{(\beta)}(S) = d\mu^{(\beta)}(S'). \quad (3.1)$$

For $\beta=1$, the transformed matrix S' is related to S by

$$S' = U_0 S U_0^T, \quad (3.2)$$

U_0 being an arbitrary, but fixed, unitary matrix. Clearly, Eq. (3.2) is an automorphism of the set of unitary symmetric matrices into itself. For $\beta=2$,

$$S' = U_0 S V_0 \quad (3.3)$$

where U_0 and V_0 are arbitrary fixed unitary matrices. For $\beta=2$, the resulting measure is the well known Haar's measure of the unitary group and its uniqueness is well known [60,61]. Uniqueness for $\beta=1$ was shown in Ref. [53]. Using the invariant measures, Eqs. (3.1) - (3.3), as the probability measures for ensembles of S -matrices defines the *Circular Orthogonal* and *Unitary Ensembles* (COE, CUE) for $\beta=1, 2$, respectively.

Several explicit representations of the invariant measure are known, the classic one being in terms of the eigenphases and eigenvectors of the S -matrix. For our purposes, the polar representation of Eq. (2.17) is of particular interest because of its connection to the conductance properties of the cavity. We thus consider the two-equal-lead case, $N_1 = N_2 = N$, and express the invariant measure explicitly in this parametrization.

We first recall a well known result from differential geometry. Consider the expression for the arc element

$$ds^2 = \sum g_{\mu\nu}(x) \delta x_\mu \delta x_\nu, \quad (3.4)$$

written in terms of *independent variables* and the metric tensor $g_{\mu\nu}(x)$. Assuming that ds^2 remains invariant under the transformation $x_\mu = x_\mu(x'_1, x'_2, \dots)$, one can prove that the volume element

$$dV = |\det g(x)|^{1/2} \prod_\mu dx_\mu \quad (3.5)$$

remains invariant under the same transformation [62].

We now go back to our random- S -matrix problem. We define the differential arc element as

$$ds^2 = \text{Tr}[dS^\dagger dS]. \quad (3.6)$$

This expression remains invariant under the transformations (3.2) and (3.3). Substituting for S the form (2.17), one can extract the metric tensor; applying Eq. (3.5), one then finds the invariant measure. This is done in A; the result is [46,63]

$$d\mu^{(\beta)}(S) = P^{(\beta)}(\{\tau\}) \prod_a d\tau_a \prod_i d\mu(v^{(i)}), \quad (3.7)$$

where $P^{(\beta)}(\{\tau\})$ denotes the joint probability density of the $\{\tau\}$, $d\mu(v^{(i)})$ is the invariant or Haar's measure on the unitary group $U(N)$ [61], and C_β is a normalization constant. From A we have

$$P^{(1)}(\{\tau\}) = C_1 \prod_{a < b} |\tau_a - \tau_b| \prod_c \frac{1}{\sqrt{\tau_c}}, \quad P^{(2)}(\{\tau\}) = C_2 \prod_{a < b} |\tau_a - \tau_b|^2. \quad (3.8)$$

Eqs. (3.7) and (3.8) explicitly specify the invariant measure. The factor involving the product over pairs gives the repulsion of the eigenvalues; notice that the repulsion is linear for the orthogonal case while quadratic in the unitary case, as typically occurs.

3.2. The information-theoretic model

3.2.1. The one-channel case To begin our discussion, consider first a physical problem that can be described by a 1×1 S matrix. This is the case, for instance, for a particle scattered by a 1D potential that is nonzero in the region $-a \leq x \leq 0$, to which an impenetrable wall is added at $x = -a$: the particle then lives in the semiinfinite domain $-a \leq x \leq \infty$. Another example is that of a 2D cavity, connected to the outside by only one lead that in turn supports only one open channel. From unitarity, S must be a complex number of unit modulus at every energy; i.e. $S(E) = e^{i\theta(E)}$. In the Argand diagram $\text{Re}(S)$ - $\text{Im}(S)$, $S(E)$ is represented, for a given energy, by a point on the unitarity circle: that point is defined by the angle $\theta(E)$. As the energy changes, so does the representative point: this is what we may call, pictorially, the “motion” of $S(E)$ as a function of energy; it resembles the motion in phase space of the representative point of a classical system as a function of time.

We ask the following question: as we move along the energy axes, *what fraction of the time do we find θ lying inside a given interval $d\theta$?* Let us call $dP(\theta) = p(\theta)d\theta$ that fraction.

To answer this question, we first analyze how to construct energy averages. By this we always mean a *local* energy average, performed inside an interval I that contains many resonances and yet is small compared to an energy interval over which “gross structure” quantities showing a secular variation, like the average spacing Δ of resonances, vary appreciably. We then expect the dependence of the average in question on the center of the interval E_0 , its width I , as well as the particular weighting function used to define the average, to be *weak*.

We devise an *idealized* situation: the argument E in $S(E)$ is extended all the way from $-\infty$ to $+\infty$, in such a way that *local averages are everywhere the same as inside I* : this idealization, which we call *stationarity*, will only represent well what goes on *locally* inside I in the actual system. We indicate an energy average of a quantity by placing a bar over it while an ensemble average is denoted by angular brackets.

Ref. [19] chooses, as the weighting function, a Lorentzian. Using the fact that $S(E)$ is *analytic* in the upper half of the complex energy plane (*causality*), it shows that

$$\overline{S^k} = [\overline{S}]^k, \quad (3.9)$$

i.e. *the average of the k -th power of S coincides with the k -th power of the average of S* . Thus, the quantity \overline{S} , referred to as the optical S matrix in Sec. 1.1, plays a special role, in that the average of any power of S can be expressed in terms of it. Ref. [19] then finds the answer to the above-posed question: the fraction of time $p(\theta)$ spent by θ in a unit interval around θ in its journey along the energy axis is *uniquely* given by the expression

$$p(\theta) = \frac{1}{2\pi} \frac{1 - |\overline{S}|^2}{|S - \overline{S}|^2}, \quad S = e^{i\theta}, \quad (3.10)$$

and *depends only upon the average, or optical, S matrix \overline{S}* . This expression is also known as *Poisson's kernel* [54]. The conclusion is remarkable: it tells us that the *system specific details are irrelevant*, except for the optical S matrix.

As an example, consider a 1D δ -potential centered at $x=0$ and a perfectly reflecting wall at $x=-a$. An energy stretch containing 100 resonances starting from $ka=10,000$ (so that secular variations of gross-structure quantities can be neglected) was sampled to find the fraction of time that θ falls in a certain small interval around θ [65]. The result is compared in Fig. 2 with Poisson's kernel (3.10),

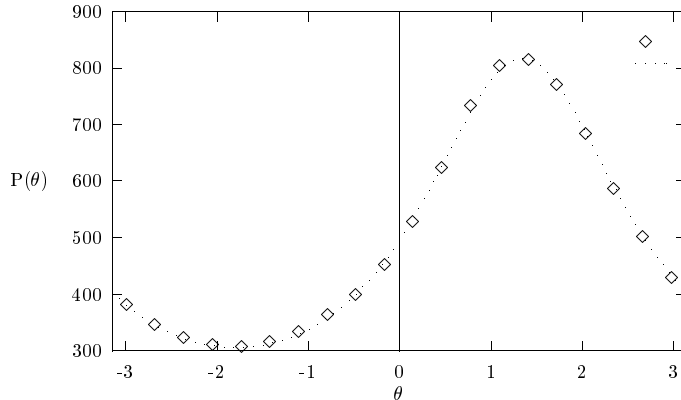


Figure 2. In the δ -potential model a stretch of energy containing 100 resonances, starting from $ka=10,000$, was sampled to find the fraction of time that θ falls in a unit interval around θ : the result is indicated by diamonds. The curve is a plot of Poisson's kernel (3.10), with the value of \bar{S} extracted from the numerical data, in order to have a parameter-free fit. The agreement is excellent. (From Ref. [65].)

where the value of the optical \bar{S} was extracted from the numerical data themselves, so as to have a parameter-free fit. We observe that the agreement is excellent.

Consider now a collection of systems, described by an ensemble of S matrices endowed with a probability measure. As an idealization, suppose we further construct $S(E)$ as a *stationary random function of energy*, for $-\infty < E < \infty$. Then we know the conditions under which *ergodicity*, understood as equality of energy and ensemble averages (except for a set of zero measure), holds [64]. Let us then assume that our ensemble is ergodic.

The condition (3.9) arising from analyticity, together with ergodicity, implies the relation

$$\langle S^k \rangle = \langle S \rangle^k \quad (3.11)$$

between ensemble averages, often called the *analyticity-ergodicity (AE)* requirement. The ensemble measure is thus *uniquely* given by

$$dP_{\langle S \rangle}(S) = p_{\langle S \rangle}(\theta) d\theta, \quad p_{\langle S \rangle}(\theta) = \frac{1}{2\pi} \frac{1 - |\langle S \rangle|^2}{|S - \langle S \rangle|^2}, \quad (3.12)$$

once $\langle S \rangle$ is specified. The ensemble depends parametrically upon the single complex number $\langle S \rangle$, *any other information being irrelevant*.

We note in passing that Eq. (3.11) implies that a function $f(S)$ that is analytic in its argument, and can thus be expanded in a power series in S , must fulfill the *reproducing property* [54,66]

$$f(\langle S \rangle) = \int f(S) dP_{\langle S \rangle}(S). \quad (3.13)$$

It is because the probability measure appears as the kernel of this integral equation that it is called Poisson's kernel.

3.2.2. The multi-channel case We now consider S matrices of dimensionality n , that can describe, in general, a multi-lead problem with n channels altogether, as explained in Sec. 2. The Argand diagram discussed above for $n=1$ has to be generalized to include the axes $\text{Re}S_{11}$, $\text{Im}S_{11}$, $\text{Re}S_{12}$, $\text{Im}S_{12}$, ..., $\text{Re}S_{nn}$, $\text{Im}S_{nn}$; S is restricted to move on the surface determined by unitarity ($SS^\dagger = I$) and, for $\beta=1$, symmetry ($S=S^T$).

We assume E is far from thresholds and recall that again $S(E)$ is *analytic* in the upper half of the complex-energy plane. The study of the statistical properties of S is again simplified by idealizing $S(E)$, for real E , as a *stationary random-matrix function* satisfying the condition of *ergodicity*. The same argument as in the 1D case above shows that the AE requirement (3.11) is generalized to

$$\langle (S_{a_1 b_1})^{n_1} \cdots (S_{a_k b_k})^{n_k} \rangle = \langle S_{a_1 b_1} \rangle^{n_1} \cdots \langle S_{a_k b_k} \rangle^{n_k}. \quad (3.14)$$

Notice that this expression involves only S , and not S^* matrix elements. Similarly, if $f(S)$ is a function that can be expanded as a series of nonnegative powers of S_{11}, \dots, S_{nn} (analytic in S), we must have the reproducing property (3.13).

Our starting point is the invariant measure $d\mu_\beta(S)$ that was introduced in the last subsection. The average of S evaluated with that measure vanishes (shown explicitly in section 4.1), so that the prompt, or direct, components described in the Introduction vanish. It is easy to check that the AE requirements (3.14) or, equivalently, the reproducing property (3.13), is satisfied exactly for the invariant measure. Ensembles that contain more information than the invariant one are constructed by multiplying the latter by appropriate functions of S . We relate the probability density $p_{\langle S \rangle}^{(\beta)}(S)$ to the differential probability through

$$dP_{\langle S \rangle}^{(\beta)}(S) = p_{\langle S \rangle}^{(\beta)}(S) d\mu_\beta(S) \quad (3.15)$$

and require the fulfillment of the AE conditions. It was shown in Ref. [66] that, for $n > 1$, the AE conditions and reality of the answer are not enough to determine the probability distribution uniquely. However, it was shown that the probability density (V_β is a normalization factor)

$$p_{\langle S \rangle}(S) = V_\beta^{-1} \frac{[\det(I - \langle S \rangle \langle S \rangle^\dagger)]^{(\beta n + 2 - \beta)/2}}{|\det(I - S \langle S \rangle^\dagger)|^{\beta n + 2 - \beta}}, \quad (3.16)$$

known again as Poisson's kernel, not only satisfies the AE requirements (3.14) [54], but the *information* \mathcal{I} associated with it

$$\mathcal{I}[p] \equiv \int p_{\langle S \rangle}(S) \ln p_{\langle S \rangle}(S) d\mu(S) \quad (3.17)$$

is *less than or equal to that of any other probability density satisfying the AE requirements for the same $\langle S \rangle$* [66]. Notice that, for $n = 1$, Eq. (3.16) reduces to (3.12). Thus the information entering Poisson's kernel specifies : **1)** General properties: *i) flux conservation* (giving rise to unitarity of the S matrix), *ii) causality* and the related analytical properties of $S(E)$ in the complex-energy plane, and *iii)* the presence or absence of time-reversal (and spin-rotation symmetry when spin is taken into account), that determines the *universality class*: orthogonal, unitary (or symplectic) **2)** A specific property: the ensemble average $\langle S \rangle$ ($= \bar{S}$ under ergodicity), which controls the presence of *prompt*, or *direct processes* in the scattering problem. System-specific *details other than the optical S are assumed to be irrelevant*.

The fact that for $n > 1$ AE and reality do not fix the ensemble uniquely is not surprising. In general (the 1×1 case being exceptional) we expect, physically, the matrix $\langle S \rangle$ to be insufficient to characterize the full distribution when, in addition to the prompt and equilibrated components, there are other contributions associated with different time scales [18]. Out of all possibilities, though, the information-theoretic argument selects the one where the prompt and equilibrated components and the associated optical S are the only physically relevant quantities.

In addition to the completely general derivation of Poisson's kernel above, we present a concrete construction of this distribution following Ref. [67,68]. For the equilibrated part of the response, suppose there is an S -matrix S_0 which is distributed according to the circular ensembles. For the prompt response, imagine a scattering process S_1 occurring prior to the response S_0 . The total scattering is the composition of these two parts. Specifically, imagine bunching the L leads of the cavity into a "superlead" containing n incoming and n outgoing waves. Along the superlead, between the cavity and infinity, we connect a scatterer of the appropriate symmetry class described by S_1 . Since there are n incoming and n outgoing waves on either side of the scatterer, S_1 is $2n$ -dimensional and can be written

$$S_1 = \begin{bmatrix} r_1 & t'_1 \\ t_1 & r'_1 \end{bmatrix}. \quad (3.18)$$

The composition of the two scattering processes yields a total S

$$S = r_1 + t'_1(1 - S_0 r'_1)^{-1} S_0 t_1. \quad (3.19)$$

One can prove [54,68,67,69] the following statement: the distribution of S is Poisson's measure (3.16) with $\langle S \rangle = r_1$ if and only if the distribution of S_0 is the invariant measure. That is, Eq. (3.19) transforms between the problem with direct processes and the one without (for the one-energy distribution considered here). Also, one can show [54,69] that the distribution is independent of the choice of t_1 and t'_1 , as long as they belong to a unitary matrix S_1 .

Note that throughout this work we use arguments which refer only to physical information expressible entirely in terms of the S -matrix. An alternate point of view is to express everything in terms of an underlying Hamiltonian which one then analyzes using statistical or information-theoretic assumptions. These two points of view give, in fact, the same results: one can prove [70,67,68] that, for $\langle S \rangle = 0$, a Gaussian Ensemble for the underlying Hamiltonian gives a Circular Ensemble for the resulting S . The argument was extended to $\langle S \rangle \neq 0$ in Refs. [67,68] using the transformation (3.19) above.

4. Absence of direct processes

In this case the optical matrix $\langle S \rangle$ vanishes and Poisson's kernel (3.16) reduces to the invariant measure:

$$dP_{\langle S \rangle=0}^{(\beta)} = d\mu^{(\beta)}(S). \quad (4.1)$$

We now derive the implications of this distribution for T , starting with the average and variance of T and then turning to its distribution.

4.1. Averages of products of S : Weak-localization and conductance fluctuations

Averages over the invariant measure of products of S matrix elements (invariant integration) can be evaluated using solely the properties of the measure, without performing any integration explicitly [20,71]. We first discuss the unitary case, because it is simpler, and then the orthogonal one.

4.1.1. The case $\beta = 2$ To illustrate the procedure, consider first the average over the invariant measure of a single S matrix element, to be denoted as

$$\langle S_{a\alpha} \rangle_0^{(2)} = \int S_{a\alpha} d\mu^{(2)}(S). \quad (4.2)$$

Even though it is trivial to recognize that this average vanishes—since the invariant measure gives the same weight to $S_{a\alpha}$ and to its negative—we present a more formal argument, which will be generalized later to more complicated averages. If U^0 is an *arbitrary* but *fixed* unitary matrix, we define the transformed \tilde{S} as

$$S = U^0 \tilde{S}. \quad (4.3)$$

Introducing (4.3) in (4.2) we have

$$\langle S_{a\alpha} \rangle_0^{(2)} = \sum_{a'} U_{aa'}^0 \int \tilde{S}_{a'\alpha} d\mu^{(2)}(\tilde{S}) = \sum_{a'} U_{aa'}^0 \langle S_{a'\alpha} \rangle_0^{(2)} \quad (4.4)$$

where we have used the defining property (3.1) of the invariant measure and the definition of $\langle S_{a'\alpha} \rangle_0$. In particular, if we take, as the arbitrary fixed matrix U^0

$$U_{aa'}^0 = e^{i\theta_a} \delta_{aa'}, \quad (4.5)$$

we find

$$\langle S_{a\alpha} \rangle_0 = e^{i\theta_a} \langle S_{a\alpha} \rangle_0. \quad (4.6)$$

Since this expression should hold for arbitrary θ_a , we conclude that

$$\langle S_{a\alpha} \rangle_0 = 0. \quad (4.7)$$

The above argument can be generalized to prove that

$$\left\langle [S_{b_1\beta_1} \cdots S_{b_p\beta_p}] [S_{a_1\alpha_1} \cdots S_{a_q\alpha_q}]^* \right\rangle_0^{(2)} = 0, \quad (4.8)$$

unless $p=q$ and unless $\{a_1, \dots, a_p\}$ and $\{b_1, \dots, b_p\}$ constitute the same set of indices except for order, with the same condition for the sets $\{\alpha_1, \dots, \alpha_p\}$, $\{\beta_1, \dots, \beta_p\}$. In particular, consider $p=q=1$. Using the same argument as above, we find

$$\langle S_{b\beta} S_{a\alpha}^* \rangle_0^{(2)} = \sum_{a'b'} U_{bb'}^0 (U_{aa'}^0)^* \langle S_{b'\beta} S_{a'\alpha}^* \rangle_0^{(2)}, \quad \forall U^0. \quad (4.9)$$

For U^0 given as in Eq. (4.5), we have

$$\langle S_{b\beta} S_{a\alpha}^* \rangle_0 = e^{i(\theta_b - \theta_a)} \langle S_{b\beta} S_{a\alpha}^* \rangle_0 \quad (4.10)$$

which vanishes unless $b=a$. Had we defined \tilde{S} through right multiplication instead of left multiplication in (4.3), we would have concluded $\beta=\alpha$. The only nonvanishing possibility in Eq. (4.9) is thus

$$\langle |S_{a\alpha}|^2 \rangle_0 = \sum_{a'} |U_{aa'}^0|^2 \langle |S_{a'\alpha}|^2 \rangle_0, \quad \forall U^0. \quad (4.11)$$

For instance, the choice of the matrix that produces a permutation of the indices 1 and 2 as U^0 yields:

$$U^0 = \begin{bmatrix} 0 & 1 & 0 & \cdots & 0 \\ 1 & 0 & 0 & \cdots & 0 \\ 0 & 0 & 1 & \cdots & 0 \\ \vdots & \vdots & \vdots & \ddots & \vdots \\ 0 & 0 & 0 & \cdots & 1 \end{bmatrix}, \quad \langle |S_{1\alpha}|^2 \rangle = \langle |S_{2\alpha}|^2 \rangle. \quad (4.12)$$

Similarly

$$\langle |S_{1\alpha}|^2 \rangle_0 = \cdots = \langle |S_{n\alpha}|^2 \rangle_0. \quad (4.13)$$

The final result for the average intensity follows from unitarity

$$\sum_{a=1}^n \langle |S_{a\alpha}|^2 \rangle_0 = 1 \quad \Rightarrow \quad \langle |S_{a\alpha}|^2 \rangle_0^{(2)} = \frac{1}{n}. \quad (4.14)$$

As an application, we calculate the *average conductance* when we have a cavity connected to the outside by means of two leads supporting N_1 and N_2 open channels (so that $n = N_1 + N_2$):

$$\langle T \rangle_0^{(2)} = \sum_{a=1}^{N_1} \sum_{b=1}^{N_2} \langle |t_{ab}|^2 \rangle_0^{(2)} = \frac{N_1 N_2}{N_1 + N_2} = \left[\frac{1}{N_1} + \frac{1}{N_2} \right]^{-1}, \quad (4.15)$$

which is the series addition of the two conductances N_1 and N_2 . (The superscript on the angular brackets indicates $\beta=2$.)

With similar arguments one finds [71]:

$$\langle |S_{12}|^2 |S_{34}|^2 \rangle_0^{(2)} = \frac{1}{n^2 - 1}, \quad (4.16)$$

$$\langle |S_{12}|^2 |S_{13}|^2 \rangle_0^{(2)} = \frac{1}{n(n+1)}, \quad (4.17)$$

$$\langle |S_{12}|^4 \rangle_0^{(2)} = \frac{2}{n(n+1)}. \quad (4.18)$$

Here, 1,2,3,4 stand for any quartet of different indices, so that n in each case must be large enough to accomodate as many indices as necessary.

As an application, we calculate the second moment of the conductance as

$$\langle T^2 \rangle_0^{(2)} = \sum_{a,c=1}^{N_1} \sum_{b,d=1}^{N_2} \langle |t_{ab}|^2 |t_{cd}|^2 \rangle_0^{(2)} = \frac{N_1^2 N_2^2}{(N_1 + N_2)^2 - 1}. \quad (4.19)$$

The variance of the conductance is then given by

$$[\text{var}(T)]_0^{(2)} = \frac{N_1^2 N_2^2}{(N_1 + N_2)^2 [(N_1 + N_2)^2 - 1]}. \quad (4.20)$$

Notice that in the limit $N_1, N_2 \rightarrow \infty$ with $N_1/N_2 = K$ fixed

$$[\text{var}(T)]_0^{(2)} \rightarrow \frac{K^2}{(K+1)^4}, \quad (4.21)$$

a constant which depends only on the ratio N_1/N_2 and on no other details of the cavity. Since this limit corresponds to increasing the width of the waveguides and so of the full system, the fact that the result is constant is the analog of the so-called *universal conductance fluctuations (UCF)* well-known for quasi-1D disordered systems [4,6]. In particular, for $K=1$, $\text{var}(T) \rightarrow 1/16$, slightly less than the quasi-1D value of $1/15$.

4.1.2. The case $\beta=1$ Just as above, we first illustrate the procedure through the average over the invariant measure of a single S matrix element [Eq. (4.2) written for $\beta=1$] which vanishes trivially. We introduce the transformed \tilde{S} , again a unitary symmetric matrix, through

$$S = U^0 \tilde{S} (U^0)^T. \quad (4.22)$$

Substituting (4.22) in the integral definition of $\langle S_{ab} \rangle_0^{(1)}$ and using the defining property of the invariant measure (3.1) we have

$$\langle S_{ab} \rangle_0^{(1)} = \sum_{a'} U_{aa'}^0 U_{bb'}^0 \int \tilde{S}_{a'b'} d\mu^{(1)}(\tilde{S}) = \sum_{a'} U_{aa'}^0 U_{bb'}^0 \langle S_{a'b'} \rangle_0^{(1)}. \quad (4.23)$$

In particular, if we take as the arbitrary fixed matrix U^0 the one given by Eq. (4.5), we find

$$\langle S_{ab} \rangle_0 = e^{i(\theta_a + \theta_b)} \langle S_{ab} \rangle_0 \implies \langle S_{ab} \rangle_0 = 0 \quad (4.24)$$

since θ_a, θ_b are arbitrary.

Just as for $\beta=2$, the above argument can be generalized to prove that

$$\left\langle [S_{a_1 b_1} \cdots S_{a_p b_p}] [S_{\alpha_1 \beta_1} \cdots S_{\alpha_q \beta_q}]^* \right\rangle_0^{(1)} = 0, \quad (4.25)$$

unless $p=q$ and unless $\{a_1, b_1, \dots, a_p, b_p\}$ and $\{\alpha_1, \beta_1, \dots, \alpha_p, \beta_p\}$ constitute the same set of indices except for order. In particular, for $p=q=1$ we find

$$\left\langle S_{ab} S_{\alpha\beta}^* \right\rangle_0^{(1)} = \sum_{a'b'\alpha'\beta'} U_{aa'}^0 U_{bb'}^0 (U_{\alpha\alpha'}^0 U_{\beta\beta'}^0)^* \left\langle S_{a'b'} S_{\alpha'\beta'}^* \right\rangle_0^{(1)}, \quad \forall U^0. \quad (4.26)$$

For instance, for U^0 given as in Eq. (4.5), we have

$$\left\langle S_{ab} S_{\alpha\beta}^* \right\rangle_0^{(1)} = e^{i(\theta_a + \theta_b - \theta_\alpha - \theta_\beta)} \left\langle S_{ab} S_{\alpha\beta}^* \right\rangle_0^{(1)}, \quad (4.27)$$

which vanishes unless $\{a, b\} = \{\alpha, \beta\}$ or $\{\beta, \alpha\}$. As a particular case, take $a=b=\alpha=\beta=1$ and, as U^0 , a matrix with the structure

$$U^0 = \begin{bmatrix} U_{11}^0 & U_{12}^0 & 0 & \cdots & 0 \\ U_{21}^0 & U_{22}^0 & 0 & \cdots & 0 \\ 0 & 0 & 1 & \cdots & 0 \\ \vdots & \vdots & \vdots & \ddots & \vdots \\ 0 & 0 & 0 & \cdots & 1 \end{bmatrix}. \quad (4.28)$$

We find

$$\begin{aligned}
\langle |S_{11}|^2 \rangle_0 &= \sum_{a'b'} U_{1a'}^0 U_{1b'}^0 (U_{1a'}^0 U_{1b'}^0)^* \langle S_{a'b'} S_{a'b'}^* \rangle_0 \\
&+ \sum_{a' \neq b'} U_{1a'}^0 U_{1b'}^0 (U_{1b'}^0 U_{1a'}^0)^* \langle S_{a'b'} S_{b'a'}^* \rangle_0 \\
&= \left[|U_{11}^0|^4 + |U_{12}^0|^4 \right] \langle |S_{11}|^2 \rangle_0 + 4 |U_{11}^0|^2 |U_{12}^0|^2 \langle |S_{12}|^2 \rangle_0.
\end{aligned} \tag{4.29}$$

Squaring the unitarity relation $|U_{11}^0|^2 + |U_{12}^0|^2 = 1$ and substituting in Eq. (4.29) we finally obtain

$$\langle |S_{11}|^2 \rangle_0^{(1)} = 2 \langle |S_{12}|^2 \rangle_0^{(1)}. \tag{4.30}$$

This result is very important. It states that time-reversal invariance (TRI) has the consequence that *the average of the absolute value squared of a diagonal S-matrix element is twice as large as that of an off-diagonal one*, under the invariant measure. By unitarity, the specific value of each one of these averages is given by

$$\langle |S_{aa}|^2 \rangle_0^{(1)} = \frac{2}{n+1}, \quad \langle |S_{a \neq b}|^2 \rangle_0^{(1)} = \frac{1}{n+1}. \tag{4.31}$$

Just as in the above case $\beta=2$, we calculate as an application the *average conductance* when our cavity is connected to the outside by two leads with N_1 and N_2 open channels ($n = N_1 + N_2$):

$$\langle T \rangle_0^{(1)} = \sum_{a=1}^{N_1} \sum_{b=1}^{N_2} \langle |t_{ab}|^2 \rangle_0^{(1)} = \frac{N_1 N_2}{N_1 + N_2 + 1}. \tag{4.32}$$

Here, the extra 1 in the denominator as compared with Eq. (4.15) is the *weak-localization correction* (WLC), a symmetry effect resulting from TRI. We can rewrite Eq. (4.32) separating out the WLC term as

$$\langle T \rangle_0^{(1)} = \frac{N_1 N_2}{N_1 + N_2} - \frac{N_1 N_2}{(N_1 + N_2)(N_1 + N_2 + 1)}. \tag{4.33}$$

In particular, for $N_1 = N_2 = N$ and for $N \rightarrow \infty$, corresponding to a large system, the WLC term tends to the universal number $-1/4$.

Using a similar procedure, one finds the results (n being again the dimensionality of the S matrix) [20]

$$\langle |S_{12}|^2 |S_{34}|^2 \rangle_0^{(1)} = \frac{n+2}{n(n+1)(n+3)}, \tag{4.34}$$

$$\langle |S_{12}|^2 |S_{13}|^2 \rangle_0^{(1)} = \frac{1}{n(n+3)}, \tag{4.35}$$

$$\langle |S_{12}|^4 \rangle_0^{(1)} = \frac{2}{n(n+3)}. \tag{4.36}$$

A comment like that made right after Eq. (4.18) applies here as well. Just as in Eq. (4.19), we now find for the second moment of the conductance

$$\langle T^2 \rangle_0^{(1)} = \frac{N_1 N_2 [N_1 N_2 (N_1 + N_2 + 2) + 2]}{(N_1 + N_2)(N_1 + N_2 + 1)(N_1 + N_2 + 3)} \tag{4.37}$$

and for its variance

$$[\text{var}(T)]_0^{(1)} = \frac{2N_1 N_2 (N_1 + 1)(N_2 + 1)}{(N_1 + N_2)(N_1 + N_2 + 1)^2 (N_1 + N_2 + 3)} \rightarrow 2 \frac{K^2}{(K+1)^4} \tag{4.38}$$

where in the limit $N_1, N_2 \rightarrow \infty$ with $N_1/N_2 = K$, a fixed number. Note that in this universal limit, the variance here is exactly twice as large as for $\beta = 2$, Eq. (4.21), another result of time-reversal invariance. For the particular case $K=1$, the limiting value of the variance is $1/8$.

4.2. The distribution of the conductance in the two-equal-lead case

In the last section we characterized the conductance of a cavity through the first two moments of its transmission. If the distribution of the conductance is Gaussian, this is sufficient to characterize the full distribution. In fact, it can be shown that in the large-size universal limit, $N \rightarrow \infty$, the distribution of the conductance is indeed Gaussian [72].

In general, however, the probability density of T will not be Gaussian, and it is of interest, then, to derive results for this density. For this purpose, the polar representation of Sec. 2.3 is particularly useful since the conductance is directly related to the $\{\tau\}$ whose joint probability distribution we know. Specifically, the distribution of the transmission T of Eq. (2.19) can be obtained by direct integration of the $P^{(\beta)}(\{\tau\})$ of Eq. (3.8):

$$w^{(\beta)}(T) = \int \delta(T - \sum_a \tau_a) P^{(\beta)}(\{\tau_a\}) \prod_a d\tau_a. \quad (4.39)$$

We consider a few examples below.

4.2.1. The case $N=1$ In this case we have only one τ_a , that we may call τ , so that $T = \tau$, and $0 \leq T \leq 1$. Eq. (3.8) then gives

$$w^{(1)}(T) = \frac{1}{2\sqrt{T}}, \quad w^{(2)}(T) = 1. \quad (4.40)$$

For $\beta=1$, we thus have a higher probability to find small T 's than $T \sim 1$: this is clearly a symmetry effect, a result of TRI that favors backscattering and hence low conductances.

4.2.2. The case $N=2$ Now $T = \tau_1 + \tau_2$, and $0 \leq T \leq 2$. In B we show that

$$w^{(1)}(T) = \begin{cases} \frac{3}{2}T, & 0 < T < 1 \\ \frac{3}{2}(T - 2\sqrt{T-1}), & 1 < T < 2 \end{cases} \quad (4.41)$$

and

$$w^{(2)}(T) = 2[1 - |1 - T|]^3 \quad (4.42)$$

For $\beta=1$, notice the square-root cusp at $T=1$. We find, once again, a higher probability for $T < 1$ than for $T > 1$ to occur. On the other hand, for $\beta=2$, $w(T)$ is again symmetric around $T=1$.

4.2.3. The case $N=3$ Now $T = \tau_1 + \tau_2 + \tau_3$, and $0 \leq T \leq 3$. For $\beta=2$ one finds

$$w^{(2)}(T) = \begin{cases} \frac{9}{42}T^8, & 0 < T < 1 \\ -\frac{2781}{14} + \frac{6588}{7}T - 1818T^2 + 1836T^3 \\ -1035T^4 + 324T^5 - 54T^6 + \frac{36}{7}T^7 - \frac{3}{7}T^8, & 1 < T < \frac{3}{2} \end{cases} \quad (4.43)$$

and the distribution is symmetric about $T=1.5$. As mentioned above, $w^{(\beta)}(T)$ gradually approaches a Gaussian distribution.

4.2.4. Arbitrary N In this case it is straightforward to obtain the dependence of the tail of the distribution in the region $0 < T < 1$. In this region the constraint that $\tau < 1$ does not enter; a calculation given in B shows that

$$w_N^{(\beta)}(T) \propto T^{\beta N^2/2-1}. \quad (4.44)$$

5. Presence of direct processes

In order to treat cases involving direct processes, as in billiards in which short paths produce a prompt response, we now need Poisson's kernel (3.16) in its full generality. We discuss below some analytical results for the distribution of the spinless conductance T in the case of a cavity connected to the outside by means of two leads supporting one open channel each ($N_1 = N_2 = 1$), giving rise to a 2-dimensional S matrix. There is only one τ in this case and it is its distribution that we seek, since $T = \tau$. While the expressions that we derive are somewhat cumbersome, they are used for comparing to numerical results in section 6 where plots of several examples are displayed.

We write the optical S -matrix \overline{S} , a subunitary matrix, as

$$\overline{S} = \begin{bmatrix} x & w \\ z & y \end{bmatrix}, \quad (5.1)$$

where the entries are, in general, complex numbers.

5.1. The case $\beta=2$

From Eq. (3.16) we write the differential probability for the S matrix as

$$dP_{\overline{S}}^{(2)}(S) = \frac{[\det(I - \overline{S}\overline{S}^\dagger)]^n}{|\det(I - S\overline{S}^\dagger)|^{2n}} d\mu_0^{(2)}(S), \quad (5.2)$$

where

$$d\mu_0^{(2)}(S) = \frac{d\mu^{(2)}(S)}{V}, \quad \int d\mu_0^{(2)}(S) = 1. \quad (5.3)$$

We are interested here in the case $n=2$.

In the polar representation (2.17) with $n=2$, the S matrix has the form

$$S = \begin{bmatrix} e^{i\alpha} & 0 \\ 0 & e^{i\beta} \end{bmatrix} \begin{bmatrix} -\sqrt{1-\tau} & \sqrt{\tau} \\ \sqrt{\tau} & \sqrt{1-\tau} \end{bmatrix} \begin{bmatrix} e^{i\gamma} & 0 \\ 0 & e^{i\delta} \end{bmatrix}, \quad (5.4)$$

the invariant measure (5.3) being [see Eqs. (3.7), (3.8)]

$$d\mu_0(S) = d\tau \frac{d\alpha d\beta d\gamma d\delta}{(2\pi)^4}. \quad (5.5)$$

1) As a particular case, suppose the optical S matrix is diagonal, so that there is *only direct reflection* and no direct transmission: in Eq. (5.1) we choose $w = z = 0$.

Substituting Eqs. (5.1), (5.4), (5.5) in (5.2) we find

$$dP_{X,Y}^{(2)}(\tau, \varphi, \psi) = \frac{(1 - X^2)^2 (1 - Y^2)^2}{|(e^{-i\varphi} + X\sqrt{1-\tau})(e^{-i\psi} - Y\sqrt{1-\tau}) - XY\tau|^4} \frac{d\tau d\varphi d\psi}{(2\pi)^2} \quad (5.6)$$

where $\varphi = \alpha + \gamma$, $\psi = \beta + \delta$, $X = |x|$, $Y = |y|$. The distribution of the conductance T is thus

$$w_{X,Y}^{(2)}(T) = (1 - X^2)^2 (1 - Y^2)^2 \times \left\langle \frac{1}{|(e^{-i\varphi} + X\sqrt{1-T})(e^{-i\psi} - Y\sqrt{1-T}) - XYT|^4} \right\rangle_{\varphi, \psi} \quad (5.7)$$

where $\langle \dots \rangle_{\varphi, \psi}$ denotes an average over the variables φ, ψ . The result is ($0 < T < 1$)

$$w_{X,Y}^{(2)}(T) = K \frac{A - B(1-T) + C(1-T)^2 + D(1-T)^3}{[E - 2F(1-T) + G(1-T)^2]^{5/2}}, \quad (5.8)$$

where

$$K = (1 - X^2)^2 (1 - Y^2)^2, \quad A = (1 - X^4 Y^4) (1 - X^2 Y^2)$$

$$\begin{aligned}
B &= (X^2 + Y^2)(1 - 6X^2Y^2 + X^4Y^4) + 4X^2Y^2(1 + X^2Y^2) \\
C &= (1 + X^2Y^2)(6X^2Y^2 - X^4 - Y^4) - 4X^2Y^2(X^2 + Y^2) \\
D &= (X^2 + Y^2)(X^2 - Y^2)^2, \quad E = (1 - X^2Y^2)^2 \\
F &= (1 + X^2Y^2)(X^2 + Y^2) - 4X^2Y^2, \quad G = (X^2 - Y^2)^2.
\end{aligned}$$

This result reduces to 1 when $X=Y=0$, as it should. A particularly interesting case is that of “equivalent channels”, i.e. $X=Y$, in which the above expression reduces to

$$w_{X,X}^{(2)}(T) = (1 - X^2) \frac{(1 - X^4)^2 + 2X^2(1 + X^4)T + 4X^4T^2}{[(1 - X^2)^2 + 4X^2T]^{5/2}}. \quad (5.9)$$

The structure of this result is clear if we notice that

$$w_{X,X}^{(2)}(0) = \left[\frac{1 + X^2}{1 - X^2} \right]^2 > 1, \quad w_{X,X}^{(2)}(1) = \frac{(1 - X^2)(1 + X^4)}{(1 + X^2)^3} < 1,$$

and hence $w_{X,X}^{(2)}(0) > w_{X,X}^{(2)}(1)$, so that small conductances are emphasized, as expected, because of the presence of direct reflection and no direct transmission.

2) The case of *only direct transmission* and no direct reflection is obtained by setting $x=y=0$ in Eq. (5.1). The conductance distribution is obtained from Eq. (5.8) with the replacement $X \rightarrow W = |w|$, $Y \rightarrow Z = |z|$, $T \rightarrow 1 - T$. In the equivalent-channel case we now obtain a conductance distribution that emphasizes large conductances.

3) The case of a general optical S matrix, Eq. (5.1), has also been worked out and the result expressed in terms of quadratures: because of its complexity, it will not be quoted here.

5.2. The case $\beta=1$

This case is more complicated than that for $\beta=2$ and we have only succeeded in treating analytically some particular cases. Take, for instance, a diagonal \bar{S} , i.e. $w=z=0$ in Eq. (5.1). With the same notation as above, we find

$$\begin{aligned}
w_{X,Y}^{(1)}(T) &= |(1 - X^2)(1 - Y^2)|^{3/2} \frac{1}{2\sqrt{T}} \\
&\times \left\langle \frac{1}{|(e^{-i\varphi} + X\sqrt{1-T})(e^{-i\psi} - Y\sqrt{1-T}) - XYT|^3} \right\rangle_{\varphi,\psi}, \quad (5.10)
\end{aligned}$$

a result that has to be integrated numerically. When $X=Y=0$, the distribution (5.11) reduces to $1/2\sqrt{T}$, as it should. It is interesting to notice that for $Y=0$ the above result can be integrated analytically, to give

$$w_{X,0}^{(1)}(T) = \frac{(1 - X^2)^{3/2}}{2\sqrt{T}} {}_2F_1(3/2, 3/2; 1; X^2(1 - T)), \quad (5.11)$$

${}_2F_1$ being a hypergeometric function [73].

6. Comparison with numerical calculations

The information-theoretic approach that we have been discussing is expected to be valid for cavities in which the classical dynamics is completely chaotic, a property that refers to the *long time* behavior of the system. It is in such structures that the long time response is ergodic and equilibrated, and so one can expect that maximum entropy considerations will play a role. In this section we examine particular cavities numerically in order to determine to what extent the information-theoretic approach really holds. The structures that we consider are all “billiards”– they consist of hard walls surrounding a cavity with constant potential– with two leads. We start by considering particularly simple structures, then treat structures in which the absence of direct processes is assured, then move on to structures having particularly obvious direct processes.

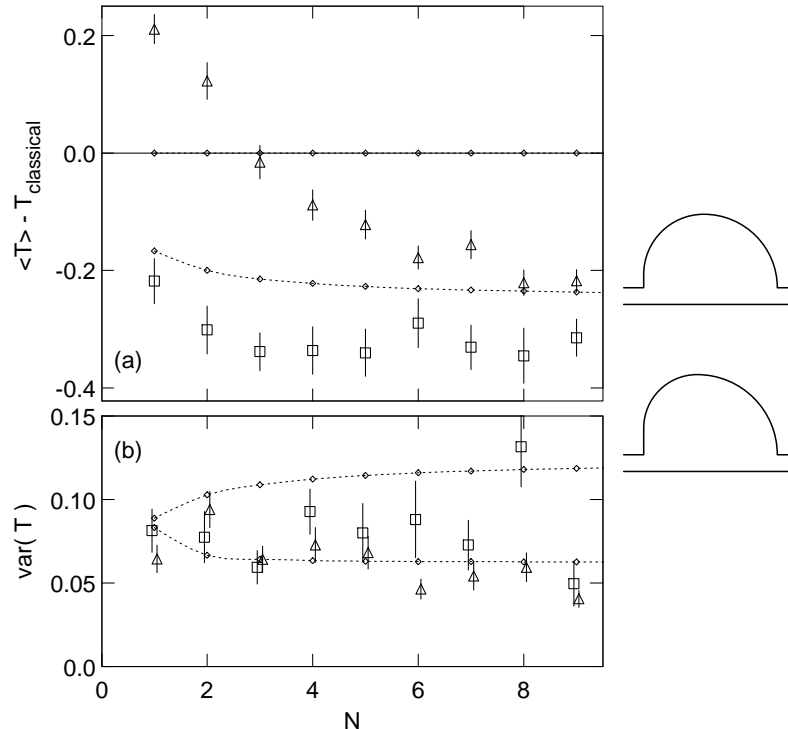


Figure 3. The magnitude of (a) the quantum correction to the classical conductance and (b) the conductance fluctuations as a function of the number of modes in the lead N . The two asymmetric stadium-like billiards shown at the right were used; the average of the results for the two cavities is shown. The numerical results for $B=0$ (squares with statistical error bars) and $B \neq 0$ (triangles) are compared to the predictions of the COE (points, dotted line) and CUE (points, dashed line). The agreement is poor. For both billiards, 25 energies were sampled for each value of N , and for non-zero field $BA/\phi_0=2, 4$ where A is the area of the cavity.

6.1. Simple structures

In the “quantum chaos” literature— the study of how quantum properties depend on the nature of the classical dynamics in a system— several billiards are used as standard examples of closed chaotic systems. The two most studied are the Sinai billiard— the region enclosed between a square and a circle centered in the square— and the stadium billiard— two half-circles joined by straight edges. The classical dynamics in these two billiards is known to be completely chaotic. For a test case open system, then, it is natural to take one of these billiards and attach two leads. The open stadium billiard was studied previously for this reason [26,32,75,76,77]. Here we directly compare results for this system to the predictions of the information-theoretic approach.

The numerical methods used in these calculations are covered in detail in Ref. [74]. Briefly, the procedure consists of the following three steps. First, discretize the Hamiltonian onto a square mesh using the simplest finite-difference scheme. Solving the Schrödinger equation is then reduced to solving a set of linear equations. Second, find the Green function at the desired energy from one lead to the other using a recursive procedure and outgoing-wave boundary conditions. This procedure essentially uses the sparseness of the finite-difference matrix to efficiently solve the linear equations. Third, note that the transmission amplitude can be obtained from this Green function by simply projecting onto the transverse wave-functions in the lead. The main parameter in these calculations, ka , is the size of the mesh compared to the wavelength. In the results shown here, ka is always less than 0.8 and $ka < 0.5$ in most cases. For these values, the anisotropy of the Fermi surface is small; the non-parabolicity of the dispersion is larger, but does not concern us here since we treat transport at a fixed energy.

Two simple quantities to calculate both numerically and theoretically are the average and variance of the conductance. The analytic results for the invariant measure are in section 4.1. Fig. 3 shows the numerical results for the two asymmetric open stadium shown on the side— asymmetric half-

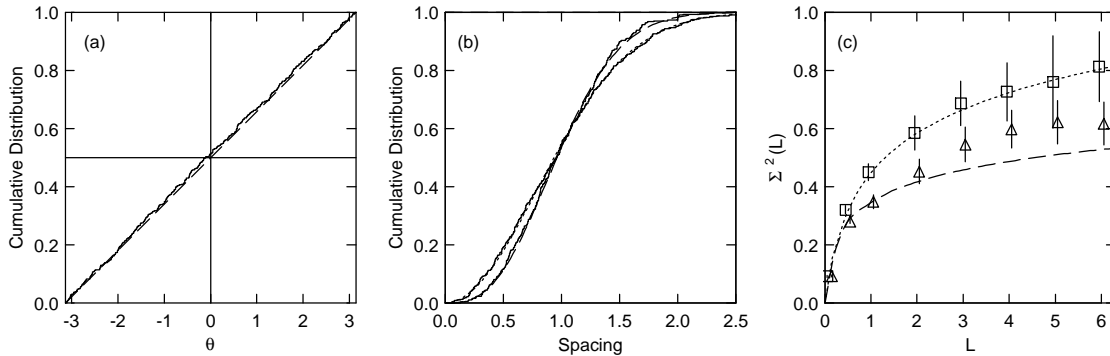


Figure 4. Statistics of the eigenphases of the S -matrix for the second stadium shown in Fig. 3 with $N = 9$. (a) Cumulative distribution of the eigenphase density (solid line) compared to the CE (dashed). (b) Cumulative distribution of the difference between nearest-neighbor phases for both $B=0$ and $BA/\phi_0 = 4$ compared to the COE (dotted) and CUE (dashed). The spacing is normalized to the mean separation. (c) Variance of number of phases in an interval L for both $B=0$ (squares) and $BA/\phi_0 = 4$ (triangles) compared to the COE (dotted) and CUE (dashed). All three statistics agree with the prediction of the circular ensembles— constant density, a spacing distribution given by the Wigner surmise, and a logarithmically increasing variance— despite the poor agreement for the transmission in Fig. 3.

stadiums are used in order to avoid the complications of reflection symmetry. The top panel shows the deviation of the average transmission from the classical value of the transmission. This classical value was obtained numerically by tracing trajectories through the cavity. For fully equilibrated scattering, the classical value is $N/2$ where N is the number of channels in each lead, but in Fig. 3 $T_{\text{classical}}/N$ is 0.60 (0.58) for the upper (lower) cavity. The bottom panel shows the variance of T . While the numerical results are similar in magnitude to the predictions, the agreement is clearly not very good.

Before proceeding with our discussion of the conductance in these cavities, we step back to perform the most common test of random matrix theory. In the context of closed systems, it is natural to consider the statistics of the energy levels. The degree to which these statistics agree with the Wigner-Dyson statistics derived from random matrix theory is often used as the prime indication of the validity of the theory for a given system. In the context of the S -matrix, the analog is to look at the statistics of the eigenphases: in the large N limit their statistics is also Wigner-Dyson [15,16]. In fact, studies of eigenphases of chaotic scattering systems were carried out prior to any interest in the conductance [23,24]. The statistics of the eigenphases can be characterized by three representative quantities [15,16]. First, the mean density of eigenphases measures the uniformity of the system; for the circular ensembles (CE) it is constant. Second, the nearest neighbor distribution highlights the repulsion at short scales; it is approximately the Wigner surmise for the CE. Third, the variance of the number of phases within a certain range L , denoted $\Sigma^2(L)$, indicates the rigidity of the spectrum at large scales; it grows logarithmically with L for the CE.

These three quantities are shown for the simple open stadium in Fig. 4. The agreement with the predictions of the CE is good for all three, in contrast to the results for the conductance above, despite N not being very large. Since the conductance involves the transmission coefficient which is a property of the wavefunctions, this indicates that the distribution of the eigenvectors is more sensitive to deviations from the CE than the distribution of eigenphases. Thus the eigenphase statistics cannot be taken as a definitive indication of the validity of the CE: it is perfectly possible to have excellent eigenvalue statistics while having poor eigenvector statistics [78].

Returning to the properties of the conductance, we believe that the deviations from the CE seen in the numerics (Fig. 3) are caused by the presence of short paths in these simple structures. This means that the response is not fully equilibrated. The two most obvious types of short paths in these structures are the direct paths between the leads and the whispering gallery paths— those that hit only the half-circle. Short paths will be included in the analysis in section 6.3 below. One way to minimize the effect of these short paths is to make the openings to the leads very small so that the probability of being trapped for a long time increases. Presumably the CE will apply to any completely chaotic

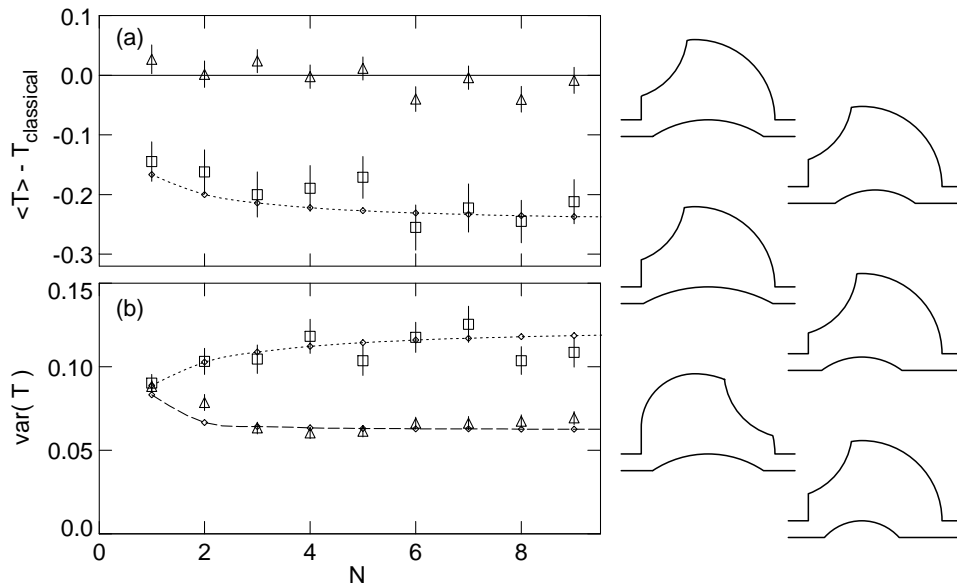


Figure 5. The magnitude of (a) the quantum correction to the classical conductance and (b) the conductance fluctuations as a function of the number of modes in the lead N . The numerical results for $B=0$ (squares with statistical error bars) agree with the prediction of the COE (points, dotted line), while those for $B \neq 0$ (triangles) agree with the CUE (points, dashed line). The six cavities shown on the right were used; the average of the numerical results is plotted. Note that each cavity has stoppers to block both the direct and whispering gallery trajectories. For non-zero field, $BA/\phi_0 = 2, 4$ where A is the area of the cavity. (After Ref. [46].)

billiard in the limit that the openings are very small (the number of modes in each lead should remain constant). However, such a structure is difficult to treat numerically, except in the very small N limit, which, in fact, we discuss in section 6.3 below.

6.2. Absence of direct processes

In order to compare with the predictions of the circular ensembles, we wish, therefore, to study structures in which the most obvious direct paths are absent. To this end, we have introduced “stoppers” into the stadium to block both the direct and the whispering gallery trajectories: examples are shown in Fig. 5. In order to study the statistical properties, the conductance as a function of energy is calculated. Because the energy variation is on the scale of $\hbar\gamma_{\text{esc}}$ (the escape rate from the cavity) [24,32], it is much more rapid than the spacing between the modes in the leads ($\hbar v_F/W$). Thus many independent samplings of the conductance at a fixed number of modes may be obtained. In addition, we vary slightly the position of the stoppers so as to change the interference effects and collect better statistics. The numerical results in Fig. 5 used 50 energies for each N (all chosen away from the threshold for the modes) and the 6 different stopper configurations shown; the classical transmission probabilities for these cavities ranged from 0.46 to 0.51 with a mean of 0.49. In addition, for non-zero magnetic field two values were used. We see that the agreement with the CE is now very good for both the mean and the variance, both for $B=0$ and for non-zero B . This supports our view that the deviations in the simple structure Fig. 3 are caused by short paths.

While the agreement of the mean and variance of the conductance with the CE gives a strong indication of the validity of the information-theoretic model for real cavities, a much more dramatic prediction of the model is the strongly non-Gaussian distribution of T for a small number of modes. The analytic results for the CE were given in section 4.2. These are compared to the numerical results for $N=1, 2$ in Fig. 6, using the same data as in Fig. 5. Note that the data is consistent with a square-root singularity in the case $N=1$ $B=0$ and with cusps in the two $N=2$ cases. Thus we see that even for this much more stringent test, the agreement between the behavior of real cavities and the CE is excellent.

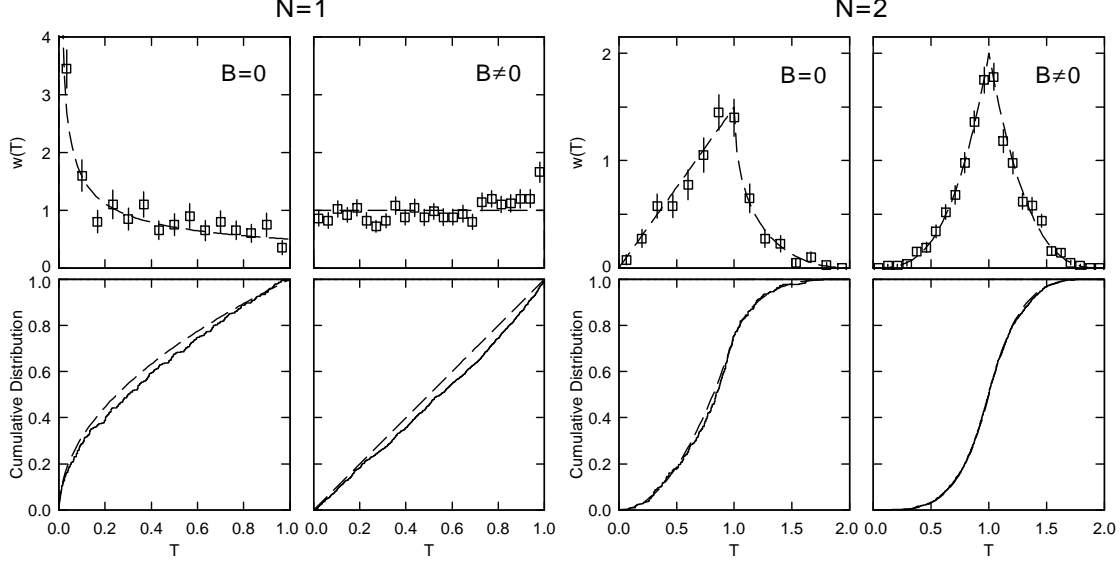


Figure 6. The distribution of the transmission intensity at fixed $N=1$ or 2 in both the absence and presence of a magnetic field, compared to the analytic COE and CUE results. The panels in the first row are histograms; those in the second row are cumulative distributions. Note both the strikingly non-Gaussian distributions and the good agreement between the numerical results and the CE in all cases. The cavities and energy sampling points used are the same as those in Fig. 5; for $B \neq 0$, $BA/\phi_0 = 2, 3, 4$, and 5 were used. (After Ref. [46].)

6.3. Presence of direct processes

We now want to look at more general structures than those used in the last section for comparing to the circular ensemble results. In particular, we will remove the stoppers that blocked short paths, and compare the numerical results with the predictions of Poisson's kernel, following Ref. [48]. We will not, however, consider the most general structure: Poisson's kernel is expected to hold in situations where there are *two* widely separated time scales, a prompt response and an equilibrated response. Thus we will study structures where we expect this to be true. Since we have only obtained explicit results in the case $N=1$ (see section 5), we will study this case numerically as well.

We have computed the conductance for several billiards shown in Fig. 7. Statistics were collected by (1) sampling in an energy window larger than the energy correlation length but smaller than the interval over which the prompt response changes, and (2) using several slightly different structures. Typically we used 200 energies in $kW/\pi \in [1.6, 1.8]$ (where W is the width of the lead) and 10 structures found by changing the height or angle of the convex “stopper”. Note that the stopper here is used to increase statistics, not block short paths. As in the absence of direct processes, since we are mostly averaging over energy, we rely on ergodicity to compare the numerical distributions to the ensemble averages of the information-theoretic model. The optical S -matrix was extracted directly from the numerical data and used as $\langle S \rangle$ in Poisson's kernel; in this sense the theoretical curves shown below are *parameter free*.

We first consider the billiard shown in Fig. 7 at low magnetic field ($BA/\phi_0 = 2$ where A is the area of the cavity; by low magnetic field we mean that the cyclotron radius r_c is much larger than the size of the cavity ($r_c = 55 W$ shown to scale). In this case $w(T)$ is nearly uniform [Fig. 7(a)], and $\langle S \rangle$ is small because direct trajectories are negligible in this large structure. We thus obtain good agreement with the invariant-measure prediction of a constant distribution (4.40).

In order to increase $\langle S \rangle$ we make one of three changes: (1) introduce potential barriers at the openings of the leads into the cavity (dashed lines in structures of Fig. 7), (2) increase the magnetic field, or (3) extend the leads into the cavity. In the first case, the barriers are chosen so that the bare transmission of each barrier is $1/2$ (determined by calculation in an infinite lead). They cause direct reflection and skew the distribution towards small T [Fig. 7(b)]. Since the reflection from the barrier is immediate while the transmitted particles are trapped for a long time, one has two very different

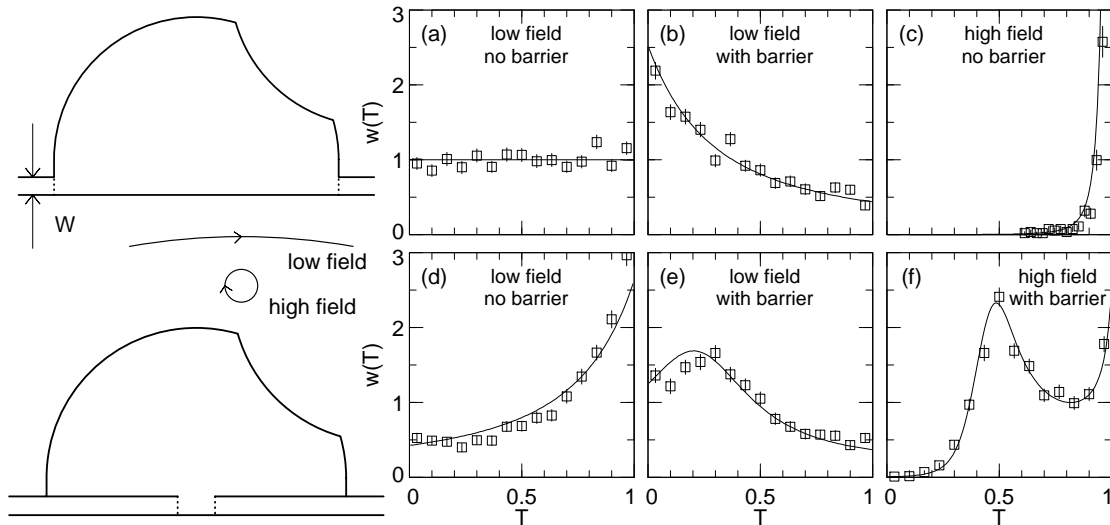


Figure 7. The distribution of the transmission coefficient for $N=1$ in a simple billiard (top row) and a billiard with leads extended into the cavity (bottom row). The magnitude of the magnetic field and the presence or absence of a potential barrier at the entrance to the leads (marked by dotted lines in the sketches of the structures) are noted in each panel. Cyclotron orbits for both fields, drawn to scale, are shown on the left. The squares with statistical error bars are the numerical results; the lines are the predictions of the information-theoretic model, parametrized by an optical S -matrix extracted from the numerical data. The agreement is good in all cases. (From Ref. [48].)

response times. Second, the large magnetic field ($BA/\phi_0=80$) corresponds to r_c just larger than the width of the lead ($r_c = 1.4 W$). The field increases one component of the direct transmission—the one corresponding to skipping orbits along the lower edge—and skews the distribution towards large T [Fig. 7(c)]. Third, extending the leads into the cavity increases the direct transmission in both directions and also skews the distribution towards large T [Fig. 7(d)]. We have done this rather than consider a smaller cavity since in our case the equilibrated component is trapped for a long time, yielding a clear separation of scales.

In each of these cases, the numerical histogram is compared to the information-theoretic model (solid lines) in which the numerically obtained \bar{S} is inserted. In panels (b)-(d) the curve plotted is the analytic expression of Eq. (5.8) and the corresponding one for direct transmission. Note the excellent agreement with the information-theoretic model.

Since the long-time classical dynamics in each of the three structures (a), (b) and (d) is chaotic, these results show that a wide variety of behavior is possible for chaotic scattering, the invariant-measure description applying only when there is a single characteristic time scale.

In case (c), the dynamics is not completely chaotic because of the small cyclotron radius, and so one would not expect the circular ensemble to apply. In Ref. [46] we found that increasing the magnetic flux through the structure beyond a few flux quanta spoiled the agreement with the circular ensemble; we now know that a nonzero $\langle S \rangle$ is generated and that the present model describes the data very well. The excellent agreement found here with a flux as high as 80 suggests extending the analysis to the quantum Hall regime.

By combining several of the modifications used above, different $\langle S \rangle$ and so different distributions can be produced. First, by using extended leads with barriers at their ends, one can cause both prompt transmission and reflection; the result is shown in Fig. 7(e). Finally, increasing the magnetic field in this structure produces a large average transmission and a large average reflection. The resulting $w(T)$, Fig. 7(f), has a surprising two-peak structure: one peak near $T=1$ caused by the large direct transmission and another near $T=1/2$. For cases (e) and (f), four intervals of 50 energies each were treated independently (since the four intervals show slightly different $\langle S \rangle$'s) and the four sets of data were then superimposed [79]. Even in these two unusual cases, the prediction of the information-theoretic model is in excellent agreement with the numerical results.

7. Comparison with experimental data: Dephasing effects

The random S -matrix theory of quantum transport through ballistic chaotic cavities was seen in the last section to be in good agreement with numerical simulations for structures in which the assumptions of the theory are expected to hold: that agreement includes the average conductance, its variance and probability density.

The ultimate test of the theory should, however, be comparisons with experiment. A naïve comparison indicates poor agreement. For instance, for $N_1 = N_2 = N = 2$, both the theoretical weak-localization correction (WLC) and variance are larger than the experimental results [38]. The theoretical WLC (including spin factor) is $-2/5 = -0.40$ from Eq. (4.33), while the experimental one is ~ -0.31 . The theoretical $\text{var}(g)$ is $4/15 \approx 0.27$ for $\beta = 2$ [Eq. (4.20)] and $72/175 \approx 0.41$ for $\beta = 1$ [Eq. (4.38)], giving the ratio $[\text{var}(g)]_0^{(1)} / [\text{var}(g)]_0^{(2)} = 54/35 \approx 1.54$. The experimental results for the variance, on the other hand, are ~ 0.015 for $B \neq 0$ and ~ 0.034 for $B = 0$, giving the ratio 2.27. In addition, the measured probability density [38] is close to a Gaussian distribution, which differs from the prediction of Eqs. (4.41), (4.42). More recent experimental data for $N = 1$ [44] show a distribution which is clearly asymmetric for $B = 0$, favoring low conductances as required by weak localization, but the asymmetry is by no means as pronounced as that of Eq. (4.40) which has a square-root singularity at the origin.

To reconcile these discrepancies, we must realize that inherent in the discussion of the previous sections is the assumption that one can neglect processes which destroy the coherence of the wave function inside the sample and neglect energy smearing caused by non-zero temperature. Even if the phase-breaking length l_ϕ is larger than the geometrical size of the cavity, for sufficiently narrow leads the electron may spend enough time inside the sample to feel the effect of phase-breaking mechanisms. The discussion of these effects and their relevance for the description of the experimental data is the subject of the present section.

We simulate the presence of phase-breaking events through a model invented by M. Büttiker [80], where, in addition to the physical leads 1,2 attached to reservoirs at chemical potentials μ_1, μ_2 , a “fake lead” 3 connects the cavity to a phase-randomizing reservoir at chemical potential μ_3 . The idea is that any particle which exits the cavity through lead 3 is replaced by a particle from the reservoir; since the replacement particle comes from a reservoir, it is incoherent with respect to the exiting particle, hence the phase-breaking. Requiring the current in lead 3 to vanish determines μ_3 ; the two-terminal dimensionless conductance is then found to be

$$g \equiv G/(e^2/h) = 2 \left[T_{21} + \frac{T_{23}T_{31}}{T_{32} + T_{31}} \right]. \quad (7.1)$$

In this equation, the factor of 2 accounts for spin explicitly and T_{ij} is the transmission coefficient for “spinless electrons” from lead j to lead i . This expression for g has a natural interpretation: the first term is the coherent transmission and the second term is the sequential transmission from 1 to 2 via 3. In terms of the S matrix, T_{ij} is

$$T_{ij} = \sum_{a_i=1}^{N_i} \sum_{b_j=1}^{N_j} \left| S_{ij}^{a_i b_j} \right|^2, \quad (7.2)$$

where N_i is the number of channels in lead i ; $S_{ij}^{a_i b_j}$ is the matrix element in the position a_i, b_j of the ij block of the S matrix, rows and columns in this block being labeled from 1 to N_i and from 1 to N_j , respectively. The total number of channels will be designated by

$$N_T = \sum_i N_i. \quad (7.3)$$

Occasionally, we shall use the notation N_ϕ to designate the number of *phase-breaking channels* N_3 in the fake lead 3. These N_ϕ channels are physically related to the phase-breaking scattering rate γ_ϕ via the relation $N_\phi/(N_1 + N_2) \approx \gamma_\phi/\gamma_{\text{esc}}$, where γ_{esc} is the escape rate from the cavity. This “fake lead” model has been used for various studies of the effect of phase-breaking in mesoscopic systems [81].

We now make the assumption that the *total* $N_T \times N_T$ scattering matrix S obeys the distribution (4.1) given by the invariant measure [47,82]. Through this assumption, the effect of the third lead is felt

somehow uniformly in space rather than at any given point. This even-handed statistical treatment makes the “fake lead” approach more physically reasonable. A further generalization to the case of non-ideal coupling of the fake lead to the cavity is studied in Ref. ([83]) but will not be presented here. In the following, we confine the analytical discussion to the large N_ϕ limit, then present the results of numerical random-matrix theory calculations, and finally compare again to experiment.

7.1. Large N_ϕ

We find below the average and variance of the conductance when $N_\phi \gg 1$ [47]. As we shall see, we need, for that purpose, the average and the covariance of the transmission coefficients T_{ij} introduced above.

From Eqs. (4.14) and (4.31), the average of T_{ij} ($i \neq j$) is given by (as usual, $\beta=1,2$)

$$\langle T_{ij} \rangle_0^{(\beta)} = \frac{N_i N_j}{N_T + \delta_{\beta 1}}, \quad (7.4)$$

so that

$$\langle T_{21} \rangle_0^{(\beta)} = \frac{N_2 N_1}{N_T + \delta_{\beta 1}} \approx \frac{N_2 N_1}{N_3} + O\left(\frac{1}{N_3^2}\right) \quad (7.5)$$

$$\langle T_{31} \rangle_0^{(\beta)} = \frac{N_3 N_1}{N_T + \delta_{\beta 1}} \approx N_1 \left[1 - \frac{N_1 + N_2 + \delta_{\beta 1}}{N_3} + O\left(\frac{1}{N_3^2}\right) \right] \quad (7.6)$$

$$\langle T_{32} \rangle_0^{(\beta)} = \frac{N_3 N_2}{N_T + \delta_{\beta 1}} \approx N_2 \left[1 - \frac{N_1 + N_2 + \delta_{\beta 1}}{N_3} + O\left(\frac{1}{N_3^2}\right) \right], \quad (7.7)$$

where the \approx sign refers to the situation $N_3 \gg 1$ while $N_1, N_2 = O(1)$. Turning to the covariance, using Eqs. (4.16)-(4.18) and (7.4), one finds for $\beta=2$

$$\langle \delta T_{ij} \delta T_{kl} \rangle_0^{(2)} = \frac{N_i N_j}{N_T^2 (N_T^2 - 1)} [N_T^2 \delta_{ik} \delta_{jl} - N_k N_T \delta_{jl} - N_l N_T \delta_{ik} + N_k N_l]. \quad (7.8)$$

Likewise, using Eqs. (4.34)-(4.36) for $\beta=1$ yields

$$\begin{aligned} \langle \delta T_{ij} \delta T_{kl} \rangle_0^{(1)} &= \frac{1}{N_T (N_T + 1)^2 (N_T + 3)} \\ &\times \{ N_i N_j (N_T + 1) (N_T + 2) (\delta_{ik} \delta_{jl} + \delta_{il} \delta_{jk}) + 2 N_i N_k \delta_{ij} \delta_{kl} \\ &+ 2 N_i N_k N_l \delta_{ij} + 2 N_i N_j N_k \delta_{kl} + 2 N_i N_T (N_T + 1) \delta_{ijkl} + 2 N_i N_j N_k N_l \\ &- (N_T + 1) [2 N_i N_l \delta_{ijk} + 2 N_i N_k \delta_{ijl} + 2 N_i N_j (\delta_{ikl} + \delta_{jkl}) \\ &+ N_i N_j N_l (\delta_{ik} + \delta_{jk}) + N_i N_j N_k (\delta_{il} + \delta_{jl})] \}. \end{aligned} \quad (7.9)$$

Here, a δ with two or more indices vanishes unless all its indices coincide, in which case its value is 1. These expressions are valid for arbitrary N_i, N_j , and also for $i=j$ if T_{ii} is interpreted as the reflection coefficient R_{ii} from lead i back to itself.

The conductance of Eq. (7.1) can be expressed as

$$\begin{aligned} g &= 2 \left[\overline{T}_{21} + \delta T_{21} + \frac{(\overline{T}_{23} + \delta T_{23}) (\overline{T}_{31} + \delta T_{31})}{(\overline{T}_{32} + \delta T_{32} + \overline{T}_{31} + \delta T_{31})} \right] \\ &= 2 \left[\overline{T}_{21} + \delta T_{21} + \frac{\overline{T}_{23} \overline{T}_{31}}{\overline{T}_{32} + \overline{T}_{31}} \frac{(1 + \delta T_{23}/\overline{T}_{23}) (1 + \delta T_{31}/\overline{T}_{31})}{1 + (\delta T_{32} + \delta T_{31})/(\overline{T}_{32} + \overline{T}_{31})} \right], \end{aligned} \quad (7.10)$$

where we have written

$$T_{ij} = \overline{T}_{ij} + \delta T_{ij}. \quad (7.11)$$

For convenience, we use interchangeably a bar or the bracket $\langle \dots \rangle_0^{(\beta)}$ to indicate an average over the invariant measure.

From Eqs. (7.8) and (7.9) we find, for the variance of T_{ij} ($i \neq j$)

$$\left\langle (\delta T_{ij})^2 \right\rangle_0^{(2)} = \frac{N_i N_j (N_T - N_i) (N_T - N_j)}{N_T^2 (N_T^2 - 1)} \quad (7.12)$$

and

$$\left\langle (\delta T_{ij})^2 \right\rangle_0^{(1)} = \frac{N_i N_j [(N_T + 1 - N_i) (N_T + 1 - N_j) - (N_T + 1) + N_i N_j]}{N_T (N_T + 1)^2 (N_T + 3)}. \quad (7.13)$$

For two leads only, i.e. for $N_\phi = 0$, these last two expressions reduce to Eqs. (4.20) and (4.38), respectively. On the other hand, for $N_\phi \gg 1$ and $i = 1, 2$

$$\frac{\left[\left\langle (\delta T_{i3})^2 \right\rangle_0^{(\beta)} \right]^{1/2}}{\bar{T}_{i3}} \sim O\left(\frac{1}{N_\phi}\right). \quad (7.14)$$

Thus, $\delta T_{23}/\bar{T}_{23}$ and $\delta T_{13}/\bar{T}_{13}$ are small quantities in Eq. (7.10), and we can make the expansion

$$\begin{aligned} g = 2 (\bar{T}_{21} + \delta T_{21}) + 2 \frac{\bar{T}_{23} \bar{T}_{31}}{\bar{T}_{32} + \bar{T}_{31}} & \left[1 + \frac{\delta T_{23}}{\bar{T}_{23}} + \frac{\delta T_{31}}{\bar{T}_{31}} - \frac{\delta T_{32} + \delta T_{31}}{\bar{T}_{32} + \bar{T}_{31}} + \frac{\delta T_{23} \delta T_{31}}{\bar{T}_{23} \bar{T}_{31}} \right. \\ & \left. + \frac{(\delta T_{23} + \delta T_{31})^2}{(\bar{T}_{32} + \bar{T}_{31})^2} - \frac{\delta T_{23} (\delta T_{32} + \delta T_{31})}{\bar{T}_{23} (\bar{T}_{32} + \bar{T}_{31})} - \frac{\delta T_{31} (\delta T_{32} + \delta T_{31})}{\bar{T}_{31} (\bar{T}_{32} + \bar{T}_{31})} + \dots \right]. \end{aligned} \quad (7.15)$$

The average of this conductance for $N_\phi \gg 1$ is obtained by using Eq. (7.14):

$$\langle g \rangle_0^{(\beta)} = 2 \left\{ \bar{T}_{21} + \frac{\bar{T}_{23} \bar{T}_{31}}{\bar{T}_{32} + \bar{T}_{31}} \left[1 + O\left(\frac{1}{N_\phi^2}\right) \right] \right\}. \quad (7.16)$$

Substituting Eqs. (7.5)-(7.7), we have

$$\langle g \rangle_0^{(\beta)} = 2 \frac{N_2 N_1}{N_2 + N_1} \left[1 - \frac{\delta_{\beta 1}}{N_\phi} \right] + O\left(\frac{1}{N_\phi^2}\right) \quad (7.17)$$

which gives the weak-localization correction

$$\delta \langle g \rangle \equiv \langle g \rangle_0^{(1)} - \langle g \rangle_0^{(2)} = -2 \frac{N_2 N_1}{N_2 + N_1} \frac{1}{N_\phi} + O\left(\frac{1}{N_\phi^2}\right). \quad (7.18)$$

Turning to the variance, we subtract the average conductance from Eq. (7.15) and obtain to lowest order in $1/N_\phi$

$$\frac{1}{2} \delta g \equiv \frac{1}{2} [g - \langle g \rangle_0^{(\beta)}] \approx \delta T_{21} + \frac{\bar{T}_{23} \bar{T}_{31}}{\bar{T}_{32} + \bar{T}_{31}} \left[\frac{\delta T_{23}}{\bar{T}_{23}} + \frac{\delta T_{31}}{\bar{T}_{31}} - \frac{\delta T_{32} + \delta T_{31}}{\bar{T}_{32} + \bar{T}_{31}} \right]. \quad (7.19)$$

and obtain, for $\beta = 1, 2$, to lowest order in $1/N_\phi$

$$\frac{1}{2} \delta g \approx \delta T_{21} + \frac{N_1}{N_2 + N_1} \delta T_{23} + \left(\frac{N_2}{N_2 + N_1} \right)^2 \delta T_{31} - \frac{N_2 N_1}{(N_2 + N_1)^2} \delta T_{32}. \quad (7.20)$$

Squaring this last expression and averaging, we obtain the variance of the conductance in terms of the $\langle \delta T_{ij} \delta T_{kl} \rangle_0$. We must now substitute the variances and covariances given in Eqs. (7.8) and (7.9) to obtain our final result:

$$[\text{var}(g)]_0^{(\beta)} = \left[\frac{2 N_2 N_1}{(N_2 + N_1) N_\phi} \right]^2 \frac{2}{\beta} \left[1 + (2 - \beta) \frac{N_2^3 + N_1^3}{N_2 N_1 (N_2 + N_1)^2} \right] + \dots \quad (7.21)$$

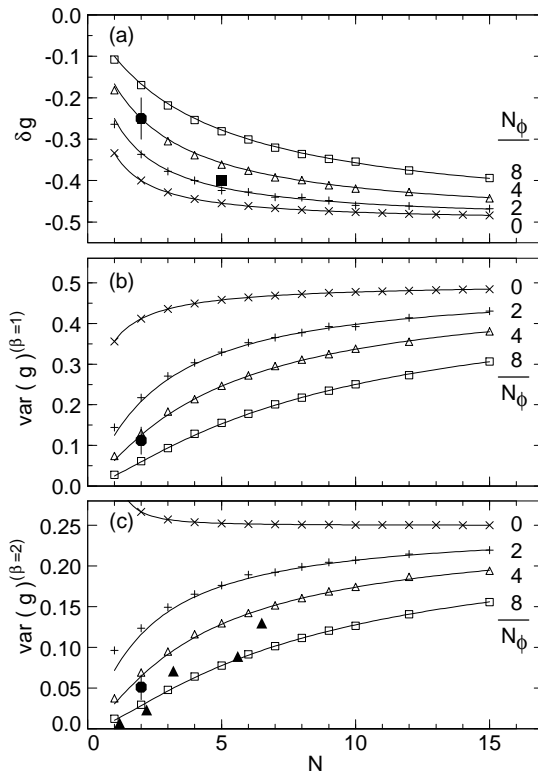


Figure 8. Magnitude of quantum transport effects as a function of the number of channels in the leads, $N_1 = N_2 = N$, for $N_\phi = 0, 2, 4$, and 8 . (a) The weak-localization correction. (b) The variance for the orthogonal case ($B=0$). (c) The variance for the unitary case (nonzero B). Open symbols are numerical results (20,000 matrices used, statistical error is the symbol size). Solid lines are interpolation formulae. Solid symbols are experimental results of Refs. [34] (squares), [35] (triangles), and [38] (circles) corrected for thermal averaging. The introduction of phase-breaking decreases the “universality” of the results but leads to good agreement with experiment. (From Ref. [47].)

The ratio of variances for $\beta=1$ and $\beta=2$ is

$$\frac{[\text{var}(g)]_0^{(1)}}{[\text{var}(g)]_0^{(2)}} = 2 \left[1 + \frac{N_2^3 + N_1^3}{N_2 N_1 (N_2 + N_1)^2} \right] + \dots \quad (7.22)$$

We observe from this last equation, first, that this ratio is independent of N_ϕ to leading order, and, second, that the ratio of variances is larger than 2, and as high as 3 for $N_2 = N_1 = N = 1$. For comparison, in the absence of phase-breaking and for $N_2 = N_1$, that ratio lies between 1 and 2.

7.2. Arbitrary N_ϕ

In order to evaluate effects of phase-breaking when N_ϕ is not large, we numerically evaluate the random-matrix theory, generating random $N_T \times N_T$ unitary or orthogonal matrices and computing g from Eq. (7.1). Fig. 8 shows the weak-localization correction and the variance of the conductance as the number of modes in the leads is varied for several fixed N_ϕ . This result is relevant to experiments at fixed temperature in which the size of the opening to the cavity is varied. Though δg and $\text{var} g$ are nearly independent of N in the perfectly coherent limit—the “universality” discussed above—phase-breaking channels cause variation. Thus the universality can be seen only if $N_\phi \ll N$; otherwise, the behavior is approximately linear.

The results of Sec. 4, which correspond to $N_\phi = 0$, and those of the last section, obtained for $N_\phi \gg 1$, suggest an approximate interpolation formula for arbitrary values of N_ϕ . For the case $N_2 = N_1 = N$, Ref. [47] proposes

$$\delta \langle g \rangle \approx -\frac{N}{2N + N_\phi} \quad (7.23)$$

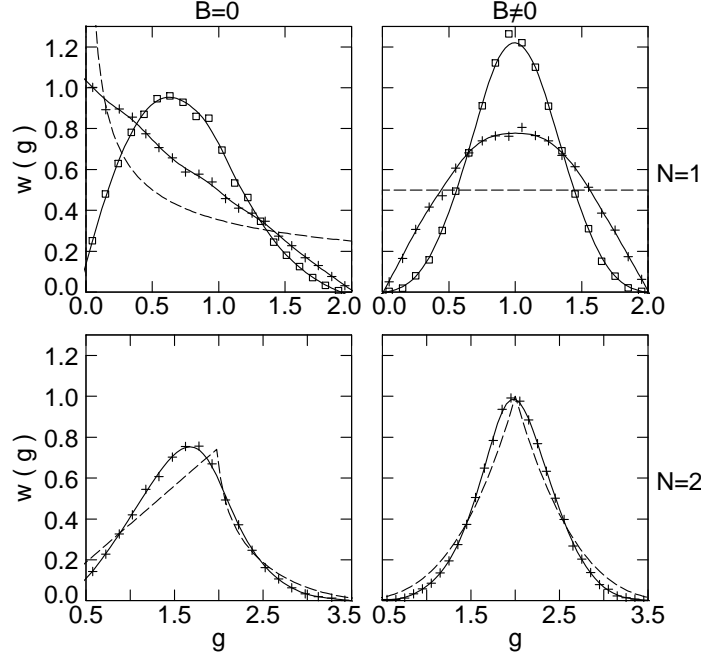


Figure 9. Probability density of the conductance in the orthogonal (first column) and unitary (second column) cases for $N = 1$ (first row) and $N = 2$ (second row). Increasing the phase-breaking from zero (dashed lines, analytic) to $N_\phi = 1$ (plus symbols, numerical) to $N_\phi = 2$ (squares, numerical) smooths the distribution. (From Ref. [47].)

for the WLC and

$$[\text{var}(g)]_0^{(\beta)} \approx \left\{ \left[[\text{var}(g)]_{0, N_\phi=0}^{(\beta)} \right]^{-1/2} + \left[[\text{var}(g)]_{0, N_\phi \gg 1}^{(\beta)} \right]^{-1/2} \right\}^{-2} \quad (7.24)$$

for the variance. These interpolation formulae are compared with the numerical simulations in Fig. 8: the agreement is good, the only significant deviation being for $N=1$ and small N_ϕ .

In addition to the mean and variance, the probability density of the conductance, $w(g)$, can be evaluated. Fig. 9 shows the distribution in the weak phase-breaking regime with a small number of modes in the lead. From the variance and mean, we know that the phase-breaking will narrow the distribution and make it more symmetric because the weak-localization correction goes to zero. Not surprisingly, the phase-breaking in addition smooths the distribution, and the extreme non-Gaussian structure in $w(g)$ is washed out.

7.3. Experiment

Now that we have a tool for evaluating the effects of phase-breaking, we return to a comparison of the information-theoretic model with experiments. First, for the mean and variance of the conductance, in Fig. 8 are also shown as black dots the results of three experiments from Refs. [34,35,38]. Since the theoretical results take into account through N_ϕ the effect of finite temperature insofar as dephasing is concerned, without including thermal smearing, the experimental variance has been corrected to compensate for this latter effect [84]. In the case of Ref. [38] measurements of all three quantum transport quantities were made, and so this data can be used to test the consistency of the theory. Notice that a value of $N_\phi = 4-8$ allows the simultaneous fit of the WLC and the variance for both $\beta = 1$ and 2. This indicates that the theory and experiment are indeed in good agreement.

Second, the full distribution of the conductance has been measured in the $N=1$ case and compared to the random-matrix theory including phase-breaking [44]. The results are shown in Fig. 10. In the $B=0$ case, the experimental distribution is clearly not Gaussian and is skewed towards small values of g , as expected. On the other hand, the distribution is not nearly as dramatic as the completely coherent theory suggests. An important recent development in relation with the fictitious lead model

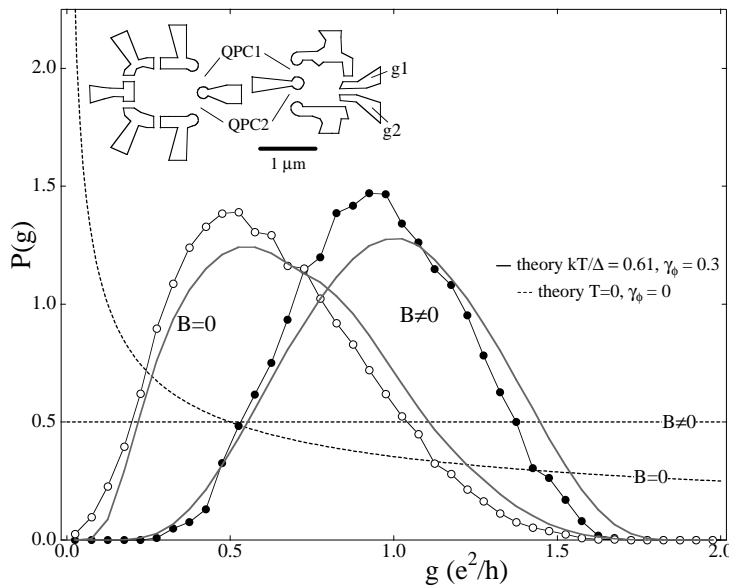


Figure 10. Experimental conductance distributions for both $B = 0$ (open circles) and 40 mT (filled circles) for a $0.5 \mu\text{m}^2$ device at 100 mK with $N=1$. These are compared to theoretical curves for both zero temperature (dashed lines) and non-zero temperature (solid lines). Though the effect of non-zero temperature is substantial, the measured distribution at $B=0$ is clearly not Gaussian. Inset: pattern of gates defining the dot. (After Ref. [44].)

described above has been carried out in Ref. [83], with the motivation of describing a spatially more uniform distribution of phase-breaking events: the fictitious lead is considered to support an infinite number of modes, each with vanishing transmission, allowing a continuous value for the dephasing rate. The experimental results are analyzed in Ref. [44] with this improved model, and the result is also shown in Fig. 10. It is seen that the shape of the conductance distribution is reproduced well with a dephasing rate obtained independently from the WLC. This comparison is strong support for the validity of the theory. The numerical value of the variance at various temperatures shows a discrepancy, though; in particular, the observed ratio of variances for $\beta=1$ and $\beta=2$ is considerably larger than that given by the model: this is as yet unexplained.

8. Conclusion

In this paper we developed a statistical theory aimed at the description of the quantum-mechanical scattering of a particle by a cavity, whose geometry is such that the classical dynamics of the system is chaotic. We studied, as our main application, the electronic transport through ballistic microstructures, in an independent-particle approximation.

The theory, which was developed in the past within nuclear physics to describe the scattering of a nucleon by a nucleus, describes the regime in which there are two distinct time scales, associated with a prompt and an equilibrated response. The prompt response is described in terms of the energy average \overline{S} —also known as the optical S matrix—of the actual S matrix. Through the notion of ergodicity, \overline{S} is calculated as the average $\langle S \rangle$ over an ensemble of similar systems, represented mathematically by an ensemble of S matrices belonging to the universality class in question: orthogonal, unitary or symplectic. In addition, the ensemble satisfies the analyticity (causality)-ergodicity requirements and the optical $\langle S \rangle$ evaluated over it has a specified (matrix) value. The ensemble discussed in the text is the one that carries minimum information, or maximum entropy, satisfying these conditions. It is thus meant to describe those situations in which any other additional information is irrelevant. In this procedure one constructs the one-energy statistical distribution of S using only the above physical information—expressible in terms of S itself—without ever invoking any statistical assumption for the underlying Hamiltonian which never enters the analysis.

From the resulting S -matrix distribution, known as Poisson's kernel, properties of the quantum conductance have been derived: its average, its fluctuations, and its full distribution in certain cases, both in the absence and presence of direct processes. We obtain good agreement with the results of the numerical solution of the Schrödinger equation for cavities in which the assumptions of the theory hold: either ones in which prompt response is absent (section 4), or ones in which there are two widely separated time scales (section 5). As for the comparison with experimental data, agreement was found once temperature smearing and dephasing effects were taken into account, at least within a phenomenological model.

The effect of time-reversal symmetry—determining the universality class β —has been seen to be of fundamental importance. One other symmetry was not touched upon in this article, because of lack of space: *spatial reflection symmetries*. While such symmetries are not relevant for disordered systems—the traditional subject of mesoscopic physics—they are possible in ballistic systems in which one can control the scattering geometry. How such symmetries affect the interference contribution to transport was studied in Refs. [85,86]. For reflection symmetries, S is block diagonal in a basis of definite parity with respect to that reflection, with a circular ensemble in each block (if $\langle S \rangle = 0$). The key point is that the conductance may couple the different parity-diagonal blocks of S , and thus the resulting quantum transport properties are a nontrivial generalization of the circular ensemble results. These effects are discussed in Ref. [85,86] for structures presenting a “left-right”, “up-down”, “four-fold”, and “inversion” spatial symmetry and compared with the results of numerical solutions of the Schrödinger equation. From an experimental point of view, it would be nice to have a confirmation of our results, both in microstructures as well as in microwave cavities, the latter ones being perhaps simpler to handle.

We should point out that the theory presented here is not applicable when there are other relevant time scales in the problem. One example is the case of a disordered quasi-1D system, where the diffusion time across the system is also an important time scale. In the past, this extra piece of information was taken into account explicitly by expressing the transfer matrix for the full system as the product of the transfer matrices for the individual slices that compose the system [87,56,88,4,7,10]. An example of an intermediate situation is that of a finite number of cavities connected in series. Whether more than two time scales are physically relevant for *single cavities* as well is not clear at present. It seems likely that the deviations of the numerical results from the theory for the simple structures in Section 6.1 are for this reason [89]. Also, it is conceivable that additional time scales are at the root of the discrepancies discussed in Ref. [85] in relation with the WLC. An extension of the maximum-entropy theory presented above to include other time scales is not known at present.

We also stress that the theory presented here is applicable to the statistics of functions of the S matrix at a single value of the energy. The joint statistical distribution of the S matrix at two or more energies has escaped, so far, an analysis within the philosophy described above (some aspects of the two-point problem have been studied assuming an underlying Hamiltonian described by a Gaussian ensemble as in Refs. [90,91]). An approach coming close to that philosophy was initiated in Ref. [92] for the simplest quantity of a two-point character: the statistical distribution of the time delay arising in the scattering process—a quantity involving the energy derivative of S —motivated by the study of the electrochemical capacitance of a mesoscopic system. It was found that another piece of information is needed for the description: the statistical distribution of the K -matrix of resonance widths. Ref. [92] deals with 1×1 S -matrices; subsequent work derived the distribution of time delays for N channels [93]. In a further development, Ref. [94] finds a transformation that relates the k -point distribution of the n -dimensional S -matrix for the case $\langle S \rangle \neq 0$ to that for $\langle S \rangle = 0$, thus relating the problems in the presence and in the absence of direct processes.

Finally, we remark that the information-theory described in the text makes use of the standard Boltzmann-Shannon definition of information and entropy. Other definitions have been presented in the literature: see, for instance, Ref. [95], and the references contained therein. What would be the physics behind the use of other definitions of entropy and how our results would be modified is not known at present.

Acknowledgments

The authors are grateful for helpful conversations with P. W. Brouwer, R. A. Jalabert, V. A. Gopar, C. M. Marcus, M. Martínez, and T. H. Seligman. PAM acknowledges partial support of CONACyT, under contract No. 2645P-E. Both authors wish to thank the hospitality of The Aspen Center for Physics, where part of this paper was developed and discussed.

A. Appendix: Evaluation of the invariant measure

We evaluate dS in the polar representation (2.17) and then the arc element ds^2 of Eq. (3.6) keeping V and W independent, as is the case for $\beta=2$. We use this same algebraic development and set $W=V^T$ in the proper place to analyze the $\beta=1$ case. Differentiating S of Eq. (2.17) we obtain

$$dS = (dV)RW + V(dR)W + VR(dW) = V[(\delta V)R + dR + R(\delta W)] \quad (\text{A.1})$$

where we have defined the matrices

$$\delta V = V^\dagger dV, \quad \delta W = (dW)W^\dagger, \quad (\text{A.2})$$

which are *antihermitian*, as can be seen by differentiating the unitarity relations $V^\dagger V = I$, $WW^\dagger = I$. The arc element of Eq. (3.6) is thus

$$\begin{aligned} ds^2 &= \text{Tr}\{[R^T(\delta V)^\dagger + dR^T + (\delta W)^\dagger R^T] \cdot [(\delta V)R + dR + R(\delta W)]\} \\ &= \text{Tr}[R^T(\delta V)^\dagger(\delta V)R + R^T(\delta V)^\dagger dR + R^T(\delta V)^\dagger R(\delta W) \\ &\quad + (dR^T)(\delta V)R + (dR^T)dR + (dR^T)R(\delta W) \\ &\quad + (\delta W)^\dagger R^T(\delta V)R + (\delta W)^\dagger R^T dR + (\delta W)^\dagger R^T R(\delta W)]. \end{aligned} \quad (\text{A.3})$$

The various differentials occurring in the previous equation can be expressed as

$$dR = \frac{1}{2} \begin{bmatrix} d\tau/\sqrt{\rho} & d\tau/\sqrt{\tau} \\ d\tau/\sqrt{\tau} & -d\tau/\sqrt{\rho} \end{bmatrix}, \quad (\text{A.4})$$

$$\delta V = \begin{bmatrix} v_1^\dagger dv_1 & 0 \\ 0 & v_2^\dagger dv_2 \end{bmatrix} = \begin{bmatrix} \delta v_1 & 0 \\ 0 & \delta v_2 \end{bmatrix}, \quad (\text{A.5})$$

$$\delta W = \begin{bmatrix} (dv_3)v_3^\dagger & 0 \\ 0 & (dv_4)v_4^\dagger \end{bmatrix} = \begin{bmatrix} \delta v_3 & 0 \\ 0 & \delta v_4 \end{bmatrix}, \quad (\text{A.6})$$

where we have used the abbreviation

$$\rho = 1 - \tau. \quad (\text{A.7})$$

We now calculate the various terms in (A.3). The first plus ninth terms give

$$\text{Tr}[(\delta V)^\dagger(\delta V) + (\delta W)^\dagger(\delta W)] = \text{Tr} \sum_{i=1}^4 (\delta v_i)^\dagger \delta v_i. \quad (\text{A.8})$$

The second plus fourth terms give

$$\begin{aligned} &\text{Tr}[R^T(\delta V)^\dagger dR + (dR^T)(\delta V)R] \\ &= \text{Tr}[\sqrt{\rho}(\delta v_1)^\dagger d\sqrt{\rho} + \sqrt{\tau}(\delta v_2)^\dagger d\sqrt{\tau} + \sqrt{\tau}(\delta v_1)^\dagger d\sqrt{\tau} + \sqrt{\rho}(\delta v_2)^\dagger d\sqrt{\rho} + h.c.] = 0, \end{aligned} \quad (\text{A.9})$$

where h.c. stands for Hermitian conjugate. We have used the identity

$$\text{Tr}[D(\delta v)^\dagger D' + D'(\delta v)D] = 0, \quad (\text{A.10})$$

where D and D' denote any two real diagonal matrices and δv an antihermitian one. Using the identity

$$\text{Tr}[(\delta v_i)^\dagger D(\delta v_j)D] = \text{Tr}[D(\delta v_j)^\dagger D(\delta v_i)], \quad (\text{A.11})$$

we find for the third plus seventh terms

$$\begin{aligned} & \text{Tr} [R^T (\delta V)^\dagger R (\delta W) + (\delta W)^\dagger R^T (\delta V) R] \\ &= 2 \text{Tr} [\sqrt{\rho} (\delta v_1)^\dagger \sqrt{\rho} (\delta v_3) + \sqrt{\tau} (\delta v_2)^\dagger \sqrt{\tau} (\delta v_3) \\ &+ \sqrt{\tau} (\delta v_1)^\dagger \sqrt{\tau} (\delta v_4) + \sqrt{\rho} (\delta v_2)^\dagger \sqrt{\rho} (\delta v_4)]. \end{aligned} \quad (\text{A.12})$$

The fifth term gives

$$\text{Tr} (dR^T) (dR) = \frac{1}{2} \sum_a \frac{(d\tau_a)^2}{\tau_a \rho_a}. \quad (\text{A.13})$$

Finally, the sixth plus eighth terms give

$$\begin{aligned} & \text{Tr} [(dR^T) R (\delta W) + h.c.] \\ &= \frac{1}{2} \text{Tr} [-(d\tau) \delta v_3 + (d\tau) \delta v_3 + (d\tau) \delta v_4 - (d\tau) \delta v_4 + h.c.] = 0. \end{aligned} \quad (\text{A.14})$$

Substituting these expressions in (A.3), we find

$$\begin{aligned} ds^2 = 2 \text{Tr} \left\{ \frac{1}{2} \sum_{i=1}^4 (\delta v_i)^\dagger (\delta v_i) + \frac{(d\tau)(d\tau)}{4\tau\rho} + \sqrt{\rho} (\delta v_1)^\dagger \sqrt{\rho} (\delta v_3) \right. \\ \left. + \sqrt{\tau} (\delta v_2)^\dagger \sqrt{\tau} (\delta v_3) + \sqrt{\tau} (\delta v_1)^\dagger \sqrt{\tau} (\delta v_4) + \sqrt{\rho} (\delta v_2)^\dagger \sqrt{\rho} (\delta v_4) \right\}. \end{aligned} \quad (\text{A.15})$$

The antihermitian matrix δv_i can be expressed as

$$\delta v_i = \delta a_i + i \delta s_i, \quad (\text{A.16})$$

where δa_i is real antisymmetric and δs_i is real symmetric. Substituting in the expression for ds^2 and rearranging terms, we find

$$\begin{aligned} ds^2 = \sum_a \left\{ \sum_{i=1}^4 ((\delta s_i)_{aa})^2 + 2\rho_a [(\delta s_1)_{aa} (\delta s_3)_{aa} + (\delta s_2)_{aa} (\delta s_4)_{aa}] \right. \\ \left. + 2\tau_a [(\delta s_2)_{aa} (\delta s_3)_{aa} + (\delta s_1)_{aa} (\delta s_4)_{aa}] + \frac{(d\tau_a)^2}{2\tau_a \rho_a} \right\} \\ + 2 \sum_{a < b} \left\{ \sum_{i=1}^4 ((\delta a_i)_{ab})^2 + \sum_{i=1}^4 ((\delta s_i)_{ab})^2 \right. \\ \left. + 2\sqrt{\rho_a \rho_b} [(\delta a_1)_{ab} (\delta a_3)_{ab} + (\delta a_2)_{ab} (\delta a_4)_{ab} + (\delta s_1)_{ab} (\delta s_3)_{ab} + (\delta s_2)_{ab} (\delta s_4)_{ab}] \right. \\ \left. + 2\sqrt{\tau_a \tau_b} [(\delta a_2)_{ab} (\delta a_3)_{ab} + (\delta a_1)_{ab} (\delta a_4)_{ab} + (\delta s_2)_{ab} (\delta s_3)_{ab} + (\delta s_1)_{ab} (\delta s_4)_{ab}] \right\}. \end{aligned} \quad (\text{A.17})$$

A.1. The case $\beta=1$

In this case, $v_3 = v_1^T$, $v_4 = v_2^T$ so $\delta v_3 = \text{deltav}_1^T$, $\delta v_4 = \text{deltav}_2^T$, and hence

$$\delta a_3 = -\delta a_1, \quad \delta s_3 = \delta s_1, \quad \delta a_4 = -\delta a_2, \quad \delta s_4 = \delta s_2. \quad (\text{A.18})$$

Substituting in (A.17), we have

$$\begin{aligned} ds^2 = 2 \sum_a \left\{ ((\delta s_1)_{aa})^2 + ((\delta s_2)_{aa})^2 + 2\tau_a (\delta s_1)_{aa} (\delta s_2)_{aa} \right. \\ \left. + \rho_a [((\delta s_1)_{aa})^2 + ((\delta s_2)_{aa})^2] + \frac{(d\tau_a)^2}{4\tau_a(1-\tau_a)} \right\} \\ + 4 \sum_{a < b} \left\{ ((\delta a_1)_{ab})^2 + ((\delta a_2)_{ab})^2 + ((\delta s_1)_{ab})^2 + ((\delta s_2)_{ab})^2 \right. \\ \left. + 2\sqrt{\tau_a \tau_b} [(\delta s_1)_{ab} (\delta s_2)_{ab} - (\delta a_1)_{ab} (\delta a_2)_{ab}] \right. \\ \left. + \sqrt{\rho_a \rho_b} [((\delta s_1)_{ab})^2 + ((\delta s_2)_{ab})^2 - ((\delta a_1)_{ab})^2 - ((\delta a_2)_{ab})^2] \right\}, \end{aligned} \quad (\text{A.19})$$

or

$$\begin{aligned}
\frac{1}{2}ds^2 = & \sum_a \left\{ (1 + \rho_a) \left[((\delta s_1)_{aa})^2 + ((\delta s_2)_{aa})^2 \right] + 2\tau_a (\delta s_1)_{aa} (\delta s_2)_{aa} + \frac{(d\tau_a)^2}{4\tau_a \rho_a} \right\} \\
& + 2 \sum_{a < b} \left\{ (1 + \sqrt{\rho_a \rho_b}) \left[((\delta s_1)_{ab})^2 + ((\delta s_2)_{ab})^2 \right] \right. \\
& \left. + (1 - \sqrt{\rho_a \rho_b}) \left[((\delta a_1)_{ab})^2 + ((\delta a_2)_{ab})^2 \right] + 2\sqrt{\tau_a \tau_b} [(\delta s_1)_{ab} (\delta s_2)_{ab} - (\delta a_1)_{ab} (\delta a_2)_{ab}] \right\}.
\end{aligned} \tag{A.20}$$

In (A.20), $(\delta s_1)_{aa}$, $(\delta s_2)_{aa}$ and τ_a ($a=1, \dots, N$) contribute N independent variations each, while $(\delta s_1)_{ab}$, $(\delta s_2)_{ab}$, $(\delta a_1)_{ab}$, $(\delta a_2)_{ab}$ ($a < b$) contribute $N(N-1)/2$ each, giving a total of

$$\nu = 3N + 4 \frac{N(N-1)}{2} = 2N^2 + N, \tag{A.21}$$

which is the correct number of independent parameters for a $2N$ -dimensional unitary symmetric matrix.

The metric tensor appearing in Eq. (3.4) has a simple block structure, consisting of 1×1 and 2×2 blocks along the diagonal, as follows. There are N 2-dimensional blocks with rows and columns labeled $(\delta s_1)_{aa}$, $(\delta s_2)_{aa}$:

$$\begin{array}{cc}
(\delta s_1)_{aa} & (\delta s_2)_{aa} \\
(\delta s_1)_{aa} & \begin{bmatrix} 1 + \rho_a & \tau_a \\ \tau_a & 1 + \rho_a \end{bmatrix} \\
(\delta s_2)_{aa} &
\end{array} \tag{A.22}$$

and N 1-dimensional blocks $1/4\rho_a\tau_a$ labeled by $d\tau_a$, giving, altogether, the contribution

$$\prod_{a=1}^N \frac{(1 + \rho_a)^2 - \tau_a^2}{4\rho_a\tau_a} = \prod_{a=1}^N \frac{1}{\tau_a} \tag{A.23}$$

to $\det g$. There are $N(N-1)/2$ 2-dimensional blocks with rows and columns labeled $(\delta s_1)_{ab}$, $(\delta s_2)_{ab}$,

$$\begin{array}{cc}
(\delta s_1)_{ab} & (\delta s_2)_{ab} \\
(\delta s_1)_{ab} & \begin{bmatrix} 1 + \sqrt{\rho_a \rho_b} & \sqrt{\tau_a \tau_b} \\ \sqrt{\tau_a \tau_b} & 1 + \sqrt{\rho_a \rho_b} \end{bmatrix} \cdot 2, \\
(\delta s_2)_{ab} &
\end{array} \tag{A.24}$$

and also $N(N-1)/2$ 2-dimensional blocks with rows and columns labeled $(\delta a_1)_{ab}$, $(\delta a_2)_{ab}$,

$$\begin{array}{cc}
(\delta a_1)_{ab} & (\delta a_2)_{ab} \\
(\delta a_1)_{ab} & \begin{bmatrix} 1 - \sqrt{\rho_a \rho_b} & -\sqrt{\tau_a \tau_b} \\ -\sqrt{\tau_a \tau_b} & 1 - \sqrt{\rho_a \rho_b} \end{bmatrix} \cdot 2, \\
(\delta a_2)_{ab} &
\end{array} \tag{A.25}$$

giving, altogether, a contribution

$$\begin{aligned}
& \left\{ \left[1 + \sqrt{(1 - \tau_a)(1 - \tau_b)} \right]^2 - \tau_a \tau_b \right\} \left\{ \left[1 - \sqrt{(1 - \tau_a)(1 - \tau_b)} \right]^2 - \tau_a \tau_b \right\} \\
& = \left[2 - \tau_a - \tau_b + 2\sqrt{(1 - \tau_a)(1 - \tau_b)} \right] \left[2 - \tau_a - \tau_b - 2\sqrt{(1 - \tau_a)(1 - \tau_b)} \right] \\
& = (\tau_a - \tau_b)^2.
\end{aligned} \tag{A.26}$$

Multiplying (A.23) and (A.26) and taking the square root, as required by Eq. (3.5), we find the result given in Eq. (3.8).

A.2. The case $\beta=2$

We go back to Eq. (A.17). We can write the single summation in that equation (except for its last term) as

$$\begin{aligned} & \sum_a \{ [(\delta s_1)_{aa} + (\delta s_3)_{aa}]^2 + [(\delta s_2)_{aa} + (\delta s_4)_{aa}]^2 - 2\tau_a [(\delta s_1)_{aa} - (\delta s_2)_{aa}] [(\delta s_3)_{aa} - (\delta s_4)_{aa}] \} \\ &= \sum_a [(\delta x_a)^2 + (\delta y_a)^2 - 2\tau_a(\delta z_a)(\delta x_a - \delta y_a - \delta z_a)], \end{aligned} \quad (\text{A.27})$$

where we have defined the combinations

$$\delta x_a = (\delta s_1)_{aa} + (\delta s_3)_{aa} \quad (\text{A.28})$$

$$\delta y_a = (\delta s_2)_{aa} + (\delta s_4)_{aa} \quad (\text{A.29})$$

$$\delta z_a = (\delta s_1)_{aa} - (\delta s_2)_{aa}. \quad (\text{A.30})$$

Notice that in ds^2 the $4N$ quantities $(\delta s_1)_{aa}, (\delta s_2)_{aa}, (\delta s_3)_{aa}, (\delta s_4)_{aa}$ appear only through the $3N$ combinations $\delta x_a, \delta y_a, \delta z_a$: these quantities, together with the $d\tau_a$ contribute $4N$ independent variations. The $(\delta s_i)_{ab}$ and the $(\delta a_i)_{ab}$ for $i=1, \dots, 4$ and $a < b$ contribute $4 \cdot N(N-1)/2$ each, so that we have a total of $4N^2$ variations, which is the correct number of independent parameters for a $2N$ -dimensional unitary matrix.

In terms of independent variations we can thus write the ds^2 of Eq. (A.17) as

$$\begin{aligned} ds^2 = & \sum_a \left\{ [(\delta x_a)^2 + (\delta y_a)^2 - 2\tau_a(\delta z_a)(\delta x_a - \delta y_a - \delta z_a)] + \frac{(d\tau_a)^2}{2\tau_a\rho_a} \right\} \\ & + 2 \sum_{a < b} \left\{ \sum_{i=1}^4 ((\delta a_i)_{ab})^2 + \sum_{i=1}^4 ((\delta s_i)_{ab})^2 \right. \end{aligned} \quad (\text{A.31})$$

$$\begin{aligned} & + 2\sqrt{\rho_a\rho_b} [(\delta a_1)_{ab}(\delta a_3)_{ab} + (\delta a_2)_{ab}(\delta a_4)_{ab} + (\delta s_1)_{ab}(\delta s_3)_{ab} + (\delta s_2)_{ab}(\delta s_4)_{ab}] \\ & + 2\sqrt{\tau_a\tau_b} [(\delta a_2)_{ab}(\delta a_3)_{ab} + (\delta a_1)_{ab}(\delta a_4)_{ab} + (\delta s_2)_{ab}(\delta s_3)_{ab} + (\delta s_1)_{ab}(\delta s_4)_{ab}] \}. \end{aligned} \quad (\text{A.32})$$

The metric tensor appearing in Eq. (3.4) has a simple block structure, consisting of 1×1 , 3×3 and 4×4 blocks along the diagonal, as follows. There are N 3-dimensional blocks with rows and columns labeled $\delta x_a, \delta y_a, \delta z_a$:

$$\begin{array}{ccc} & \delta x_a & \delta y_a & \delta z_a \\ \begin{array}{c} \delta x_a \\ \delta y_a \\ \delta z_a \end{array} & \begin{bmatrix} 1 & 0 & -\tau_a \\ 0 & 1 & \tau_a \\ -\tau_a & \tau_a & 2\tau_a \end{bmatrix} \end{array} \quad (\text{A.33})$$

and N 1-dimensional blocks $1/2\rho_a\tau_a$ labeled by $d\tau_a$, giving, altogether, the contribution

$$\prod_{a=1}^N \frac{2\tau_a(1-\tau_a)}{2\tau_a(1-\tau_a)} = 1 \quad (\text{A.34})$$

to $\det g$. There are $N(N-1)/2$ 4-dimensional blocks with rows and columns labeled $(\delta s_1)_{ab}, (\delta s_2)_{ab}, (\delta s_3)_{ab}, (\delta s_4)_{ab}$ (for $a < b$)

$$\begin{array}{cccc} & (\delta s_1)_{ab} & (\delta s_2)_{ab} & (\delta s_3)_{ab} & (\delta s_4)_{ab} \\ \begin{array}{c} (\delta s_1)_{ab} \\ (\delta s_2)_{ab} \\ (\delta s_3)_{ab} \\ (\delta s_4)_{ab} \end{array} & \begin{bmatrix} 1 & 0 & \sqrt{\rho_a\rho_b} & \sqrt{\tau_a\tau_b} \\ 0 & 1 & \sqrt{\tau_a\tau_b} & \sqrt{\rho_a\rho_b} \\ \sqrt{\rho_a\rho_b} & \sqrt{\tau_a\tau_b} & 1 & 0 \\ \sqrt{\tau_a\tau_b} & \sqrt{\rho_a\rho_b} & 0 & 1 \end{bmatrix} \end{array} \quad (\text{A.35})$$

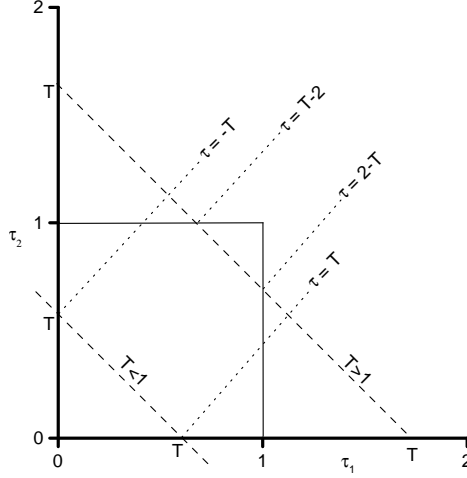


Figure B1. Region of integration for finding the distribution $w(T)$ in the $N = 2$ case.

and also $N(N-1)/2$ 4-dimensional blocks with rows and columns labeled $(\delta a_1)_{ab}$, $(\delta a_2)_{ab}$, $(\delta a_3)_{ab}$, $(\delta a_4)_{ab}$ and identical to the matrices of (A.35) giving, altogether, a contribution

$$(\tau_a - \tau_b)^4. \quad (\text{A.36})$$

Multiplying (A.34) and (A.36) and taking the square root, as required by Eq. (3.5), we find the result given in Eq. (3.8).

B. Appendix: The distribution of the conductance in the absence of direct processes

We derive here the two-channel conductance distribution of Eqs. (4.41) and (4.42) and the behavior of that distribution for arbitrary N in the range $0 < T < 1$, as given by Eq. (4.44).

For the two-channel distribution we have to perform the integral (4.39) in the two-dimensional space τ_1, τ_2 , inside the square $0 < \tau_1 < 1, 0 < \tau_2 < 1$, indicated in Fig. B1. The change of variables

$$T = \tau_1 + \tau_2, \quad \tau = \tau_1 - \tau_2 \quad (\text{B.1})$$

will be found advantageous. As shown in Fig. B1, when $0 < T < 1$ the variable τ varies in the interval $-T < \tau < T$, whereas when $1 < T < 2$ we have $T-2 < \tau < 2-T$.

B.1. Derivation of Eq.(4.42).

From Eq. (3.8) for the invariant measure we find, for two channels

$$P^{(2)}(\tau_1, \tau_2) = C (\tau_1 - \tau_2)^2. \quad (\text{B.2})$$

The normalization constant is found from

$$1 = C \int_0^1 \int_0^1 (\tau_1 - \tau_2)^2 d\tau_1 d\tau_2 = \frac{C}{2} \left[\int_0^1 dT \int_{-T}^T d\tau \cdot \tau^2 + \int_1^2 dT \int_{T-2}^{2-T} d\tau \cdot \tau^2 \right] = \frac{C}{6}, \quad (\text{B.3})$$

so that $C=6$.

The distribution of the spinless conductance is thus

$$w^{(2)}(T) = 3 \left[\int_0^1 dT' \delta(T - T') \int_{-T'}^{T'} d\tau \cdot \tau^2 + \int_1^2 dT' \delta(T - T') \int_{T'-2}^{2-T'} d\tau \cdot \tau^2 \right], \quad (\text{B.4})$$

so that

$$w^{(2)}(T < 1) = 2T^3, \quad w^{(2)}(1 < T < 2) = 2(2-T)^3. \quad (\text{B.5})$$

These two equations can be condensed in the result of Eq. (4.42).

B.2. Derivation of Eq. (4.41)

From Eq. (3.8) for the invariant measure we find, for two channels

$$P^{(1)}(\tau_1, \tau_2) = C \frac{|\tau_1 - \tau_2|}{\sqrt{\tau_1 \tau_2}}. \quad (\text{B.6})$$

The normalization constant is found from

$$\begin{aligned} 1 &= C \int \int_0^1 \frac{|\tau_1 - \tau_2|}{\sqrt{\tau_1 \tau_2}} d\tau_1 d\tau_2 \\ &= \frac{C}{2} \left[\int_0^1 dT \int_{-T}^T d\tau \frac{2|\tau|}{\sqrt{T^2 - \tau^2}} + \int_1^2 dT \int_{T-2}^{2-T} d\tau \frac{2|\tau|}{\sqrt{T^2 - \tau^2}} \right] = \frac{4}{3}C, \end{aligned} \quad (\text{B.7})$$

so that $C=3/4$.

The distribution of the spinless conductance is thus

$$\begin{aligned} w^{(1)}(T) &= \frac{3}{8} \left[\int_0^1 dT' \delta(T - T') \int_{-T'}^{T'} d\tau \frac{2|\tau|}{\sqrt{(T')^2 - \tau^2}} \right. \\ &\quad \left. + \int_1^2 dT' \delta(T - T') \int_{T'-2}^{2-T'} d\tau \frac{2|\tau|}{\sqrt{(T')^2 - \tau^2}} \right], \end{aligned} \quad (\text{B.8})$$

so that

$$w^{(1)}(T < 1) = \frac{3}{2}T, \quad w^{(1)}(1 < T < 2) = \frac{3}{2} \left[T - 2\sqrt{T-1} \right], \quad (\text{B.9})$$

which are Eqs. (4.41) we wanted to prove.

B.3. Derivation of Eq. (4.44)

The integration region selected by the δ function in Eq. (4.39) is $N-1$ dimensional. In the particular case $T < 1$, each of the τ_a 's ($a=1, \dots, N$) varies, over that region, in the interval $0 < \tau_a < T$. This is clearly illustrated in Fig. B1 for $N=2$, where the relevant region is the segment extending from $(\tau_1, \tau_2) = (0, T)$ to $(\tau_1, \tau_2) = (T, 0)$. For $T < 1$ the corners of the N -dimensional hypercube are not relevant; they become relevant for $T > 1$. We can thus write, for $T < 1$

$$w_N^{(\beta)}(T < 1) = C_N^{(\beta)} \int_0^T \cdots \int_0^T \delta \left(T - \sum_{a=1}^N \tau_a \right) \prod_{a < b} |\tau_a - \tau_b|^\beta \prod_c \tau_c^{\frac{\beta-2}{2}} \prod_i d\tau_i \quad (\text{B.10})$$

Introducing the new variables $\sigma_a = \tau_a/T$ ($a=1, \dots, N$) which vary in the interval $(0, 1)$, we have

$$\begin{aligned} w_N^{(\beta)}(T < 1) &= C_N^{(\beta)} \int_0^1 \cdots \int_0^1 \delta \left(T - T \sum_{a=1}^N \sigma_a \right) T^{\frac{N(N-1)}{2}\beta} \prod_{a < b} |\sigma_a - \sigma_b|^\beta T^{N\frac{\beta-2}{2}} \prod_c \sigma_c^{\frac{\beta-2}{2}} T^N \prod_i d\sigma_i \\ &= C_N^{(\beta)} T^{\beta\frac{N^2}{2}-1} \int_0^1 \cdots \int_0^1 \delta \left(1 - \sum_{a=1}^N \sigma_a \right) \prod_{a < b} |\sigma_a - \sigma_b|^\beta \prod_c \sigma_c^{\frac{\beta-2}{2}} \prod_i d\sigma_i, \end{aligned} \quad (\text{B.11})$$

which behaves as the power of T indicated in Eq. (4.44).

References

- [1] R. G. Newton, *Scattering Theory of Waves and Particles* (Springer-Verlag, New York, 1982).
- [2] H. C. van de Hulst, *Light Scattering from Small Particles* (Dover, New York, 1981).
- [3] P. Sheng, *Scattering and Localization of Classical Waves in Random Media* (World Scientific, Singapore, 1990).
- [4] B. L. Altshuler, P. A. Lee and R. A. Webb, eds., *Mesoscopic Phenomena in Solids* (North-Holland, Amsterdam, 1991).
- [5] H. Feshbach, *Theoretical Nuclear Physics— Nuclear Reactions* (Wiley, New York, 1992).
- [6] C. W. J. Beenakker and H. van Houten in *Solid State Physics*, edited by H. Ehrenreich and D. Turnbull (Academic, New York, 1991), Vol. 44, pp. 1-228.
- [7] *Mesoscopic Quantum Physics*, edited by E. Akkermans, G. Montambaux, J.-L. Pichard, and J. Zinn-Justin (Elsevier, New York, 1995).
- [8] *Mesoscopic Electron Transport*, edited by L. L. Sohn, L. P. Kouwenhoven, and G. Schön (Kluwer Academic, Boston, 1997).
- [9] *Nanotechnology*, edited by G. L. Timp, (Springer-Verlag, New York, 1998).
- [10] C. W. J. Beenakker, *Rev. Mod. Phys.* **69**, 731 (1997).
- [11] *Chaos and Quantum Physics*, edited by M.-J. Giannoni, A. Voros, and J. Zinn-Justin (North-Holland, New York, 1991).
- [12] M. C. Gutzwiller, *Chaos in Classical and Quantum Mechanics* (Springer Verlag, New York, 1991).
- [13] H. Feshbach, C. E. Porter and V. F. Weisskopf, *Phys. Rev.* **96**, 448 (1954).
- [14] H. Feshbach, *Topics in the Theory of Nuclear Reactions*, in *Reaction Dynamics* (Gordon and Breach, New York, 1973).
- [15] M. L. Mehta, *Random Matrices* (Academic, New York, 1991).
- [16] C. E. Porter, *Statistical Theories of Spectra: Fluctuations* (Academic, New York, 1965).
- [17] J. B. French, P. A. Mello and A. Pandey, *Phys. Lett. B* **80**, 17 (1978).
- [18] D. Agassi, H. A. Weidenmüller and G. Mantzouranis, *Phys. Rep.* **22**, 145 (1975).
- [19] G. López, P. A. Mello and T. H. Seligman, *Z. Phys. A* **302**, 351 (1981).
- [20] P. A. Mello and T. H. Seligman, *Nucl. Phys. A* **344**, 489 (1980).
- [21] R. D. Levine, *Quantum Mechanics of Molecular Rate Processes* (Oxford University Press, Oxford, 1969), Ch. 3.5; W. J. Miller, *J. Chem. Phys.* **65**, 2216 (1976).
- [22] T. Ericson and T. Mayer-Kuckuk, *Ann. Rev. Nucl. Sc.* **16**, 183 (1966).
- [23] M. C. Gutzwiller, *Physica D* **7**, 341 (1983).
- [24] R. Blümel and U. Smilansky, *Phys. Rev. Lett.* **60**, 477 (1988); *Physica D* **36**, 111 (1989); *Phys. Rev. Lett.* **64**, 241 (1990).
- [25] For a review of classical and quantum chaotic scattering see U. Smilansky in Ref. [11] pp. 371-441.
- [26] E. Doron, U. Smilansky, and A. Frenkel, *Phys. Rev. Lett.* **65**, 3072 (1990); *Physica D* **50**, 367 (1991).
- [27] J. Stein, H.-J. Stöckmann, and U. Stoffregen, *Phys. Rev. Lett.* **75**, 53 (1995) and references therein.
- [28] A. Kudrolli, V. Kidambi, and S. Sridhar, *Phys. Rev. Lett.* **75**, 822 (1995) and references therein.
- [29] H. Alt, A. Bäcker, C. Dembowski, H.-D. Gräf, R. Hofferbert, H. Rehfeld, and A. Richter, *Phys. Rev. E* **58**, 1737 (1998) and references therein.
- [30] M. Stoytchev and A. Z. Genack, *Phys. Rev. Lett.* **79**, 309 (1997) and references therein.
- [31] M. E. Gertsenshtein and V. B. Vasil'ev, *Theor. Probab. Appl.* **4**, 391 (1959); **5**, 340(e) (1960) [*Teor. Veroyatn. Primen.* **4**, 424 (1959); **5**, 3(E) (1960)].
- [32] R. A. Jalabert, H. U. Baranger, and A. D. Stone, *Phys. Rev. Lett.* **65**, 2442 (1990).
- [33] C. M. Marcus, R. M. Westervelt, P. F. Hopkins, and A. C. Gossard, *Phys. Rev. B* **48**, 2460 (1993).
- [34] A. M. Chang, H. U. Baranger, L. N. Pfeiffer, and K. W. West, *Phys. Rev. Lett.* **73**, 2111 (1994).
- [35] M. J. Berry, J. A. Katine, R. M. Westervelt, and A. C. Gossard, *Phys. Rev. B* **50**, 17721 (1994); M. J. Berry, J. H. Baskey, R. M. Westervelt and A. C. Gossard, *Phys. Rev. B* **50**, 8857 (1994).
- [36] J. P. Bird, K. Ishibashi, Y. Aoyagi, T. Sugano, and Y. Ochiai, *Phys. Rev. B* **50**, 18678 (1994).
- [37] M. W. Keller, A. Mittal, J. W. Sleight, R. G. Wheeler, D. E. Prober, R. N. Sacks, H. Shtrikmann, *Phys. Rev. B* **53**, R1693 (1996).
- [38] I. H. Chan, R. M. Clarke, C. M. Marcus, K. Campman and A. C. Gossard, *Phys. Rev. Lett.* **74**, 3876 (1995).
- [39] G. Lütjering, K. Richter, D. Weiss, J. Mao, R. H. Blick, K. von Klitzing, and C. T. Foxon, *Surf. Sci.* **361**, 709 (1996).
- [40] I. V. Zozoulenko, R. Schuster, K.-F. Berggren, and K. Ensslin, *Phys. Rev. B* **55**, R10209 (1997).
- [41] Y. Lee, G. Faini, and D. Mailly, *Phys. Rev. B* **56**, 9805 (1997).
- [42] A. S. Sachrajda, R. Ketzmerick, C. Gould, Y. Feng, P. J. Kelly, A. Delage, and Z. Wasilewski, *Phys. Rev. Lett.* **80**, 1948 (1998).
- [43] L. Christensson, H. Linke, P. Omling, P. E. Lindelof, I. V. Zozoulenko, and K.-F. Berggren, *Phys. Rev. B* **57**, 12306 (1998).
- [44] A. G. Huibers, S. R. Patel, C. M. Marcus, P. W. Brouwer, C. I. Duruöz, and J. S. Harris, Jr., *Phys. Rev. Lett.* **81**, 1917 (1998) [cond-mat/9801174].
- [45] For reviews of the semiclassical treatment of ballistic cavities see A. D. Stone in Ref. [7] and H. U. Baranger in Ref. [9].
- [46] H. U. Baranger and P. A. Mello, *Phys. Rev. Lett.* **73**, 142 (1994).
- [47] H. U. Baranger and P. A. Mello, *Phys. Rev. B* **51**, 4703 (1995).
- [48] H. U. Baranger and P. A. Mello, *Europhys. Lett.* **33**, 465 (1996).
- [49] H. U. Baranger and A. D. Stone, *Phys. Rev. B* **40**, 8169 (1989).

- [50] K. W. McVoy, Nuclear Resonance Reactions and S-Matrix Analyticity, in *Fundamentals in Nuclear Theory* (International Atomic Energy Agency, Vienna, 1967).
- [51] A. M. Lane and R. G. Thomas, Rev. Mod. Phys. **30**, 257 (1958).
- [52] E. Merzbacher, *Quantum Mechanics*, 2nd. Ed., J. Wiley 1970.
- [53] F. J. Dyson, J. Math. Phys. **3**, 140 (1962).
- [54] L. K. Hua, *Harmonic Analysis of Functions of Several Complex Variables in the Classical Domains*, translated by L. Ebner and A. Koranyi (Amer. Math. Soc., Providence RI, 1963).
- [55] P. A. Mello and J.-L. Pichard, J. Phys. I **1**, 493 (1991).
- [56] P. A. Mello, P. Pereyra and N. Kumar, Ann. Phys. (N.Y.) **181**, 290 (1988).
- [57] M. Büttiker, IBM Jour. Res. Develop. **32**, 317 (1988).
- [58] Y. B. Levinson, Zh. Eksp. Teor. Fiz. **95**, 2175 (1989) [Sov. Phys. JETP **68**, 1257 (1989)].
- [59] Y. B. Levinson and B. Shapiro, Phys. Rev. B **46**, 15520 (1992).
- [60] E. P. Wigner, *Group Theory and its Applications to the Quantum Mechanics of Atomic Spectra* (Academic Press, New York, 1959).
- [61] M. Hamermesh, *Group Theory and Its Applications to Physical Problems* (Addison-Wesley, Reading MA, 1962), p. 313.
- [62] H. Lass, *Vector and Tensor Analysis* (McGraw-Hill, New York, 1950) p. 277, Ex. 125; pp. 279, 280; p. 287, Pr. 7.
- [63] R. A. Jalabert, J.-L. Pichard and C. W. J. Beenakker, Europhys. Lett. **27**, 255 (1994).
- [64] A. M. Yaglom, *An Introduction to the Theory of Stationary Random Functions* translated by R. A. Silverman (Prentice-Hall, New York, 1962).
- [65] V. A. Gopar, Ph. D. Thesis, Universidad Nacional Autónoma de México, México, 1999.
- [66] P. A. Mello, P. Pereyra and T. H. Seligman, Ann. Phys. (N.Y.) **161**, 276 (1985).
- [67] P. W. Brouwer, Phys. Rev. B **51**, 16878 (1995).
- [68] P. W. Brouwer, *On the Random-Matrix Theory of Quantum Transport*, Doctoral Thesis, University of Leiden, 1997.
- [69] W. Friedman and P. A. Mello, Ann. Phys. (N.Y.) **161**, 276 (1985).
- [70] H. Nishioka and H. A. Weidenmüller, Phys. Lett. B **157**, 101 (1985); S. Iida, H. A. Weidenmüller and J. A. Zuk, Ann. Phys. (N.Y.) **200**, 219 (1990); C. H. Lewenkopf and H. A. Weidenmüller, Ann. Phys. (N.Y.) **212**, 53 (1991).
- [71] P. A. Mello, J. Phys. A **23**, 4061 (1990).
- [72] H. D. Politzer, Phys. Rev. B **40**, 11917 (1989).
- [73] M. Abramowitz and I. E. Stegun, *Handbook of Mathematical Functions* (National Bureau of Standards, Washington, 1964) Ch. 15.
- [74] H. U. Baranger, D. P. DiVincenzo, R. A. Jalabert, and A. D. Stone, Phys. Rev. B **44**, 10637 (1991).
- [75] R. Jensen, Chaos **1**, 101 (1991).
- [76] H. U. Baranger, R. A. Jalabert, and A. D. Stone, Phys. Rev. B **70**, 3876 (1993).
- [77] H. U. Baranger, R. A. Jalabert, and A. D. Stone, Chaos **3**, 665 (1993).
- [78] The same effect has been noticed in the context of random matrix Hamiltonians: one can have Gaussian ensemble eigenvalue statistics while not having Porter-Thomas wavefunction statistics (E. Mucciolo, private communication).
- [79] While $\langle S \rangle$ varies slightly over the full energy range used, the distribution of T implied by $\langle S \rangle$ does not vary. Thus, the theoretical curve shown in Fig. 7 is the average of the prediction of Poisson's kernel for each of the four intervals of 50 energies. The numerical result is the histogram of all of the data.
- [80] M. Büttiker, Phys. Rev. B **33** 3020 (1986).
- [81] Previous uses of the "fake lead" approach to dephasing include S. Datta, Phys. Rev. B **40**, 5830 (1989); G. Kirzenow, Solid State Commun. **74**, 1051 (1990); J. L. D'Amato and H. M. Pastawski, Phys. Rev. **41**, 7441 (1990); S. Hershfield, Phys. Rev. B **43**, 11586 (1991); D. P. DiVincenzo, Phys. Rev. B **48**, 1404 (1993).
- [82] P. W. Brouwer and C. W. J. Beenakker, Phys. Rev. B **51**, 7739 (1995).
- [83] P. W. Brouwer and C. W. J. Beenakker, Phys. Rev. B **55**, 4695 (1997).
- [84] To compensate for the thermal smearing in the experiment, we estimate the energy correlation length E_c from the data given and then multiply the experimental variance by $3.5kT/E_c$. For [38], this produces a factor of ~ 2.6 -4.5.
- [85] H. U. Baranger and P. A. Mello, Phys. Rev. B **54**, R14297 (1996).
- [86] V. A. Gopar, M. Martínez, P. A. Mello, and H. U. Baranger, J. Phys. A **29**, 881 (1996).
- [87] O. N. Dorokhov, Pis'ma Zh. Eksp. Teor. Fiz. **36**, 259 (1982) [JETP Lett. **36**, 318 (1982)].
- [88] P. A. Mello and A. D. Stone, Phys. Rev. B **44**, 3559 (1991).
- [89] For the simple structures of section 6.1, in addition to comparing the numerical results to the invariant-measure theory, we also compared to Poisson's kernel. The agreement was also poor in this case because the statistics were not stationary so that an optical S -matrix could not be unambiguously defined. In contrast, the structures of section 6.3 have smaller openings: this causes two widely separated time scales, and so Poisson's kernel is a good description.
- [90] C. Lewenkopf and H. A. Weidenmüller, Ann. Phys. (N.Y.) **212**, 53 (1991).
- [91] Y. V. Fyodorov and H.-J. Sommers, J. Math. Phys. **38**, 1918 (1997).
- [92] V. Gopar, P. A. Mello and M. Büttiker, Phys. Rev. Lett. **77**, 3005 (1996).
- [93] P. W. Brouwer, K. M. Frahm, and C. W. J. Beenakker, Phys. Rev. Lett. **78**, 4737 (1997) and cond-mat/9809022.
- [94] V. A. Gopar and P. A. Mello, Europhys. Lett. **42**, 131 (1998).
- [95] C. Tsallis, J. Stat. Phys. **52**, 479 (1988); Physica A **221**, 277 (1995).